

# The orientation of disk galaxies around large cosmic voids.

Jesús Varela

Juan Betancort-Rijo

Ignacio Trujillo  
and

Elena Ricciardelli

*Instituto de Astrofísica de Canarias (IAC), E-38200 La Laguna, Tenerife, Spain*  
*Depto. Astrofísica, Universidad de La Laguna (ULL), E-38206 La Laguna, Tenerife, Spain*

April 26, 2019

## ABSTRACT

Using a large sample of galaxies from the SDSS-DR7, we have analysed the alignment of disk galaxies around cosmic voids. We have constructed a complete sample of cosmic voids (devoid of galaxies brighter than  $M_r - 5 \log h = -20.17$ ) with radii larger than  $10 h^{-1}$  Mpc up to redshift 0.12. Disk galaxies in shells around these voids have been used to look for particular alignments between the angular momentum of the galaxies and the radial direction of the voids. We find that disk galaxies around voids larger than  $\geq 15 h^{-1}$  Mpc within distances not much larger than  $5 h^{-1}$  Mpc from the surface of the voids present a significant tendency to have their angular momenta aligned with the void's radial direction with a significance  $\geq 98.8\%$  against the null hypothesis. The strength of this alignment is dependent on the void's radius and for voids with  $\lesssim 15 h^{-1}$  Mpc the distribution of the orientation of the galaxies is compatible with a random distribution. Finally, we find that this trend observed in the alignment of galaxies is similar to the one observed for the minor axis of dark matter halos around cosmic voids found in cosmological simulations, suggesting a possible link in the evolution of both components.

*Subject headings:* Large Scale Structure: Voids; Galaxies : General

## 1. Introduction

The study of the alignment of galaxies with respect to the large scale structure is a recurrent topic still not fully settled. The first works studying the alignment of galaxies focused on clusters and superclusters. Studies on the alignment of galaxies in clusters (Adams et al. 1980) and superclusters (Flin & Godlowski 1986; Kashikawa & Okamura 1992) claimed to find particular alignments of the galaxies with respect to their local large scale structure. On the other side, similar studies did not find any particular alignment (Helou & Salpeter 1982; Dekel 1985; Garrido et al. 1993). More

recently, Navarro et al. (2004) revisited the analysis done by Flin & Godlowski (1986) on the alignment of galaxies in the Local Supercluster (LSC) under the light of the Tidal Torque Theory (for a recent review about the Tidal Torque Theory or TTT, see Schäfer 2009). The authors found a tendency of galaxies to have their spin parallel to the plane of the LSC, also known as supergalactic plane, that would support the predictions from the TTT.

However, the observational analysis is hindered by two main difficulties: the accurate determination of the direction of the angular momentum of the galaxies and the determination of the distribution of matter around

them. The determination of the spin of disk galaxies can be guessed by the shape of the galaxy, considering that galaxies spin around their minor axis. However, there is still an indetermination due to projection effects since in most of the cases it is not possible to know which half, of the two in which a galaxy is divided by its major axis, is closer to the observer. The presence of dust lanes or the use of kinematic data can help to solve this degeneracy but in most of the cases this information is not available. To deal with this problem some authors have taken all the possibilities of the spin as independent ones (Kashikawa & Okamura 1992) while others have opted for taking just one possibility (Lee & Erdogdu 2007).

Regarding the accurate determination of the mass distribution around the galaxies, the main problem comes from the effects of the proper motion of galaxies which introduces uncertainties in the conversion from redshift to distances.

To overcome both problems, Trujillo et al. (2006, hereafter T06) proposed the use of spiral galaxies seen edge-on or face-on (so the direction of the spin vector is better determined) located in the shells around cosmic voids. The advantage of the regions around large cosmic voids is that the direction of the gradient of density is strongly aligned with the radial direction which can be determined in a robust way despite the uncertainties of converting redshifts in distances. Using this technique and data from the third data release of the Sloan Digital Sky Survey (SDSS-DR3) and the 2dF Galaxy Redshift Survey (2dFGRS), T06 found a tendency of galaxies around shells of voids to have their spin vector perpendicular to the radial direction. Cuesta et al. (2008) working on cosmological simulations of dark matter halos around voids found results in apparent agreement with those of T06. The simulations show that the angular momentum of the dark matter halos tend to be also aligned to the perpendicular direction. In both cases, the results were in agreement with the prediction done using the TTT (Lee & Pen 2000), that the angular momentum would tend to be aligned with the intermediate axis of the tidal shear tensor, that in the surface of the voids is in the perpendicular direction.

However, recently, Slosar & White (2009, hereafter S09) have redone a similar analysis, but using a larger sample of galaxies from the SDSS-DR6, obtaining a result that is consistent with a random distribution of orientations, in contrast with the previous results.

In this work, we revisit the analysis of the alignment

of galaxies around voids with two significant improvements with respect to those two previous works. First, we make use of the latest data release of the SDSS, i.e. SDSS-DR7, and we combine it with the morphological classification from the Galaxy Zoo project (Banerji et al. 2010; Lintott et al. 2010) to select disk galaxies. Second, we have developed a statistical procedure to partially correct the indetermination in the spin direction due to the projection effect so we can obtain information also from galaxies that are not edge-on or face-on, increasing by a factor of 3 the effective number of galaxies that are used in our analysis with respect to the restriction to edge-on and face-on galaxies.

The outline of this Paper is as follows. Section 2 presents the data used for our analysis; Section 3 describes the procedure to search for voids; Section 4 is devoted to the selection of galaxies and the computation of their alignments; Section 5 contains the final results; in Section 6 the results are discussed and compared with previous works and in Section 7 the summary of the results are presented.

Through this paper we assume a  $\Lambda$ CDM cosmological model with  $\Omega_M = 0.3$ ,  $\Omega_\Lambda = 0.7$  and  $H_0 = 100 h \text{ km s}^{-1} \text{ Mpc}^{-1}$ .

## 2. The data

On what follows we describe the data that we have used to: a) create a sample of cosmic voids, and b) obtain a sample of galaxies in the shells surrounding them to explore the orientation of galaxies in the large scale structure.

Our main source of data has been the New York University Value-Added Galaxy Catalog<sup>1</sup>(NYU-VACG, Blanton et al. 2005; Padmanabhan et al. 2008; Adelman-McCarthy et al. 2008), which is based on the photometric and spectroscopic catalog of the SDSS-DR7<sup>2</sup> (Strauss et al. 2002). The main characteristics of the NYU-VACG are:

- Spectroscopically complete up to  $r \sim 17.8$  (extinction corrected)
  - Completeness  $\sim 99\%$
  - Success rate  $\sim 99.9\%$
- $\mu_{50}(r - \text{band}) \leq 24.5 \text{ mag arcsec}^{-2}$

<sup>1</sup><http://sdss.physics.nyu.edu/vagc/>

<sup>2</sup><http://cas.sdss.org/astrodr7/en/>

- $\sim 90$  targets/deg<sup>2</sup>
- Median( $z$ )=0.104

## 2.1. Selection of the sample of galaxies

We have established thresholds in absolute magnitude,  $M_r^{lim}$ , and redshift,  $z^{lim}$ , in order to maximize the amount of galaxies while keeping the final sample complete in spectroscopy. The completeness of the initial catalog is a basic requirement to avoid the detection of spurious voids.

In Figure 1 it is plotted the number of galaxies with  $M_r \leq M_r^{lim}(z)$  as a function of the redshift. The value of  $M_r^{lim}(z)$  corresponds to completeness limit ( $r = 17.8$ ) at each redshift  $z$ . From the peak of this distribution we obtain the limits of our final sample:

- $z \leq 0.12$
- $M_r - 5 \log h \leq -20.17^3$

## 2.2. Volume trimming

Although we focus our analysis in the largest continuous volume of SDSS-DR7, the irregular limits of the volume still posed difficulties in the reliable detection of voids. For this reason, we have defined new regular limits minimizing the detection of spurious voids while still keeping  $\sim 90\%$  of the original volume.

Figure 2 shows the limits of our trimmed volume, projected onto the original distribution of galaxies, defined as follows:

- $\delta > 0^\circ$  [Southern limit]
- $\delta < -2.555556(\alpha - 131^\circ)$  [Western limit]
- $\delta < 1.70909(\alpha - 235^\circ)$  [Eastern limit]
- $\delta < \arcsin\left[\frac{0.93232 \sin(\alpha - 95.9^\circ)}{\sqrt{1 - [0.93232 \cos(\alpha - 95.9^\circ)]^2}}\right]$  [Northern limit]

Table 1 summarizes the main properties of the reference catalog that we have used in our search for cosmic voids.

<sup>3</sup>We opted for no applying a k-correction due to the small redshift range probe and the high uncertainties in its determination.

## 2.3. Homogeneity check

Another important requirement of the galaxy catalog to be suitable to search for voids is the homogeneity. One common test of homogeneity is the  $\langle V/V_{max} \rangle$  test, for which a value of 0.5 is expected for an homogenous distribution.

To perform this test, first of all, for each galaxy it is computed the volume,  $V$ , of the sphere with radius the distance along the line-of-sight to it. Then, the maximum of all the volumes,  $V_{max}$ , is found and the ratio  $V/V_{max}$  is obtained for each galaxy. The final step is to calculate the average value of these ratios,  $\langle V/V_{max} \rangle$ .

For our galaxy catalog  $\langle V/V_{max} \rangle = 0.49990$ , confirming that at large scale the distribution of galaxies in our volume is homogeneous.

## 3. Catalog of voids

With the catalog of galaxies described in the previous section, we proceed to search for cosmic voids on it. In this section we describe the procedure followed to construct our catalog of voids.

### 3.1. Procedure description

First of all, we need to establish the definition of “void” that we use in our analysis. We have opted for the simplest one: a spherical volume devoid of any galaxy brighter than our completeness limit. This definition has been already used in other works such as Patiri et al. (2006a), Patiri et al. (2006b), Trujillo et al. (2006), Brunino et al. (2007), and Cuesta et al. (2008). Cuesta et al. (2008) found that for dark matter haloes in cosmological simulations, using ellipsoidal voids instead of spherical ones does not affect significantly their results. This gives us confidence in the use of spherical voids for our analysis.

Apart from minor differences, the procedure that we have followed is basically the HB VOID FINDER described in Patiri et al. (2006a). These are the basic steps:

1. Random points are thrown within the volume of the catalog.
2. For each trial point, the 4 closest galaxies are found and the center and radius of the sphere defined by these 4 galaxies are computed and stored.
3. Of the resulting spheres, those fulfilling any of the following criteria are rejected:

Reference catalog	NYU-VAGC (Galaxies)
Spectroscopic completeness limit	$r \leq 17.8$
Redshift limits	$0.005 < z < 0.12$
Absolute magnitude limit	$M_r - 5 \log h \leq -20.17$
Number of galaxies	142127
Total Projected Area	1.941484 strad
	$0.1545 \times 4\pi$
Total Volume	$0.0276556 (h^{-1} \text{ Gpc})^3$
Average density of galaxies	$0.00514 (h^{-1} \text{ Mpc})^{-3}$

Table 1: Summary of properties of the reference catalog.

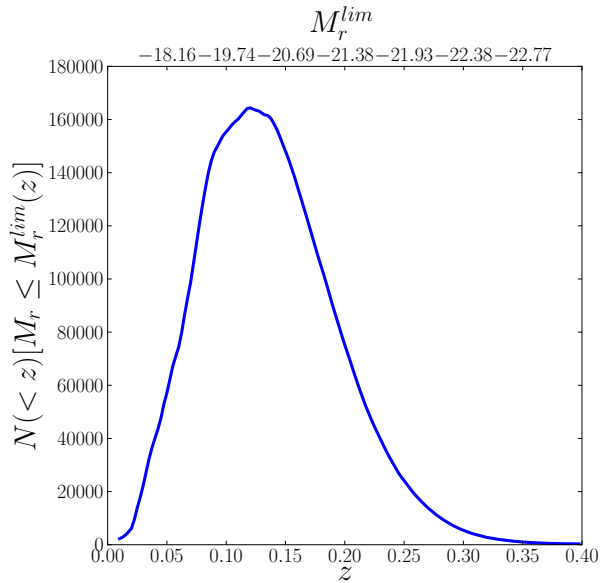


Fig. 1.— Number of galaxies brighter than  $M_r^{lim}$  with  $z < z^{lim}$ .  $M_r^{lim}$  is the absolute magnitude corresponding to the spectroscopic limit ( $r = 17.8$ ) at redshift  $z^{lim}$ . The peak of the distribution it is used to establish the thresholds in  $M_r$  and  $z$  of our initial catalog.

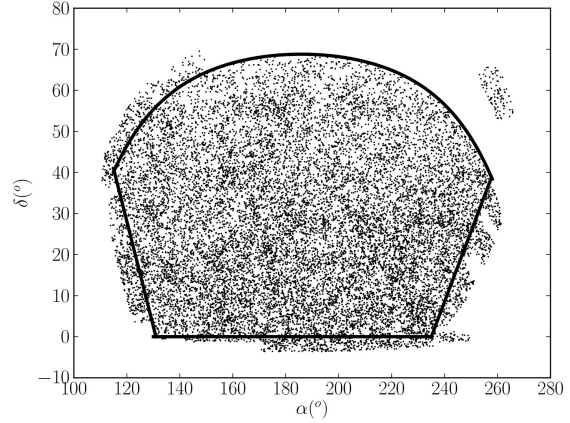


Fig. 2.— Partial projection of galaxies from the SDSS-NYU catalog. The limits used in this work are overlotted.

- Not being empty.
- Intersecting the border of the volume.<sup>4</sup>
- Having a radius smaller than  $10 h^{-1} \text{ Mpc}$ .

Finally, to have well defined spherical voids, we impose that they can not overlap. In the case in which several voids overlap, only the largest one is kept. The order in which the rejection of the voids is done affects their final sample. Therefore, to ensure that our final sample contains the largest possible voids, the process of rejection of overlapping voids it is done from the largest void to the smallest one.

<sup>4</sup>Patiri et al. (2006a) used a different technique. They put artificial galaxies in the limits of the survey, allowing voids to be defined by three real galaxies and one fake one.

In summary, the voids selected for our final catalogs fulfill the following conditions:

1. They are empty of galaxies from the initial catalog, i.e.  $M_r < -20.17 + 5 \log h$ .
2. Their radius is larger than  $10 h^{-1}$  Mpc.
3. They are completely inside the surveyed volume.<sup>5</sup>
4. Voids do not overlap, i.e. the distance between the centers of two voids is larger than the sum of their radii.

The power of this procedure to produce a complete catalog of voids depends critically on the relation between the density of galaxies, the size of the voids and the number of trial points used in the search. We have performed several tests and have found that using  $\sim 10^9$  initial random points (corresponding to a density of  $\sim 35 (h^{-1} \text{Mpc})^{-3}$  trial points) ensures that the completeness of our catalog of voids is  $> 99\%$ .

The final outcome of this procedure is a complete catalog of 699 non-overlapping cosmic voids with radius larger than  $10 h^{-1}$  Mpc. We found a median radius of  $11.85 h^{-1}$  Mpc and the average density of voids is  $32.2 \times 10^{-3} (h^{-1} \text{Mpc})^{-3}$ .<sup>6</sup>

Table 2 provides the main information of these voids. For each void, we include the position of the center, both in Cartesian coordinates  $(X, Y, Z)$ , and equatorial coordinates  $(\alpha, \delta)$  and redshift  $z$ ; and the radius  $(R)$ . The Cartesian coordinates are computed as follows:

$$\begin{aligned} X &= D(z) \cos \delta \cos \alpha \\ Y &= D(z) \cos \delta \sin \alpha \\ Z &= D(z) \sin \delta \end{aligned}$$

where  $D(z)$  is the comoving radial distance.

#### 4. Catalog of galaxies in shells around voids

Using the previous catalog of voids, we extract those galaxies within shells of  $10 h^{-1}$  Mpc around each of them. The morphology of the galaxies has been

<sup>5</sup>Be aware that this criterion implies that the effective volume in which the center of voids can reside is smaller than the whole volume and depends on the sizes of the voids.

<sup>6</sup>Density computed within the effective volume in which the centers of the voids can be located.

obtained from the Galaxy Zoo catalog (Banerji et al. 2010; Lintott et al. 2010), which provides robust distinction between elliptical and disk galaxies, although  $\sim 52\%$  of the galaxies remain classified as “uncertain”. We select only those galaxies classified as “spiral” in the Galaxy Zoo catalog ( $\sim 37\%$ ) because for them the direction of the angular momentum is well defined by their minor axes.

This results in a final sample of 45522 measurements, from 32374 single galaxies, that has been used to study the alignment of their angular momentum with respect to the void.<sup>7</sup> The use of measurements of galaxies falling in more than one shell is justified because the small uncertainties introduced are compensated by the increase in the size of the sample.

In the following sections we describe in detail how this alignment has been computed.

#### 4.1. Computation of the alignment

The advantage of studying galaxies around voids is that, on average, the density increases radially. This makes the radial direction a good proxy for the distribution of matter around each galaxy. Therefore, we use the minor axis of the galaxies to define the orientation of their angular momentum, and the radial direction of the voids to characterize the distribution of matter around them. Hence, our analysis is focused on the angle between these two directions,  $\theta$ .<sup>8</sup> For practical reasons, in the context of this work we will use the expression “radial direction” to mean the direction defined by a galaxy and the center of the corresponding void, and “perpendicular direction” to mean any direction perpendicular to the radial direction.

To compute the angle  $\theta$  we need to define the direction of the angular momentum or spin,  $s$ , of each galaxy. We do this, first of all, by computing the inclination angle between the plane of the galaxy disk and the line of sight,  $\zeta$ . Following Haynes & Giovanelli (1984) and Lee & Erdogdu (2007)<sup>9</sup>, we use a model of thick disk with a projected minor-to-major axis ratio  $a/b$  and an intrinsic flatness  $f$  (i.e. the ratio between the real minor axis and the real major axis). According

<sup>7</sup>These data is available upon request to the authors.

<sup>8</sup>A schematic illustration of this method is shown in Figure 1 of T06.

<sup>9</sup>Lee & Erdogdu (2007) used the angle  $i$  defined as the angle between the plane of the galaxy and the projected plane of the sky, therefore  $\zeta = \pi/2 - i$ .

$X$ [ $h^{-1}$ Mpc]	$Y$ [ $h^{-1}$ Mpc]	$Z$ [ $h^{-1}$ Mpc]	$R$ [ $h^{-1}$ Mpc]	$\alpha$ [deg]	$\delta$ [deg]	$z$
-193.463	-145.544	193.384	18.703	216.954492	38.617468	0.1059
-227.081	26.372	140.238	18.205	173.375602	31.526741	0.0914
-226.366	17.375	175.425	18.104	175.610699	37.692842	0.0979
-86.105	93.444	136.020	17.606	132.659407	46.949188	0.0630

Table 2: Catalog of voids (excerpt). Complete version in electronic form. See text for more details.

to this model,  $\zeta$  can be obtained applying the formula:

$$\sin^2 \zeta = \frac{(b/a)^2 - f^2}{1 - f^2} \quad (1)$$

For values of  $b/a < f$ , the angle is set to 0.

The flatness  $f$  depends on the morphological type of the galaxies and we use an average value of 0.14.

From Equation (1) it is easy to see that to a single value of  $b/a$  corresponds two values of  $\zeta$ :  $\zeta_+ = |\zeta|$  and  $\zeta_- = -|\zeta|$ . The indetermination is irrelevant for  $\zeta = 0$  (edge-on galaxies) and for  $\zeta = \pm\pi/2$  (face-on galaxies).

To compute the spin vector  $\mathbf{s}$  we followed the prescription by T06. According to this, if  $(\alpha, \delta)$  are the equatorial coordinates of a galaxy,  $\zeta$  the inclination angle obtained from Equation (1) and  $\phi$  is the position angle of the galaxy increasing counterclockwise (i.e. from north to east in the plane of the sky), the components of  $\mathbf{s}$  are:

$$s_x = \cos \alpha \cos \delta \sin \zeta + \cos \zeta (\sin \phi \cos \alpha \sin \delta - \cos \phi \sin \alpha) \quad (2)$$

$$s_y = \sin \alpha \cos \delta \sin \zeta + \cos \zeta (\sin \phi \sin \alpha \sin \delta + \cos \phi \cos \alpha) \quad (3)$$

$$s_z = \sin \delta \sin \zeta - \cos \zeta \sin \phi \cos \delta \quad (4)$$

Next, we compute the angle between the radial vector that connects the center of the void,  $\mathbf{r}_{void}$ , with the center of the galaxy,  $\mathbf{r}_{galaxy}$ :

$$\mathbf{r} = \mathbf{r}_{galaxy} - \mathbf{r}_{void}. \quad (5)$$

Having obtained  $\mathbf{r}$  and  $\mathbf{s}$ , the angle between them,  $\theta$ , it is computed as:

$$\theta = \arccos \left( \frac{\mathbf{s} \cdot \mathbf{r}}{|\mathbf{s}| |\mathbf{r}|} \right) \quad (6)$$

## 4.2. Analytical model of the distribution of $\theta$

We compute the angle  $\theta$  for all the galaxies in our sample of galaxies around voids, obtaining a distribution of  $\theta$ . Betancort-Rijo & Trujillo (2009) provide an analytical model for the distribution of the angle  $\theta$ , or to be more precise, of  $|\cos \theta|$ ,  $P(|\cos \theta|)$ . From theoretical principles confirmed by simulations, the authors found that  $P(|\cos \theta|)$  is well described by the expression:

$$P(\mu) = \frac{p du}{[1 + (p^2 - 1)\mu^2]^{3/2}}; \mu \equiv |\cos \theta|, \quad (7)$$

where  $p$  is a free parameter that describes the overall shape of the probability distribution. An interesting property of this distribution is the relation between the parameter  $p$  and the average value of  $|\cos \theta|$ :

$$p = \frac{1}{\langle |\cos \theta| \rangle} - 1 \quad (8)$$

Besides, the values of  $p$  are related with the existence or absence of particular alignment between the vectors  $\mathbf{r}$  and  $\mathbf{s}$  according to the following criteria:

$p < 1$ .  $\mathbf{r}$  and  $\mathbf{s}$  tend to be parallel.

$p = 1$ . There is no particular alignment between  $\mathbf{r}$  and  $\mathbf{s}$ .

$p > 1$ .  $\mathbf{r}$  and  $\mathbf{s}$  tend to be perpendicular.

It has been found that Equation (7) describes well the results from cosmological simulations (Brunino et al. 2007; Cuesta et al. 2008).

An alternative expression for the same distribution described by Equation (7) it is provided by Lee (2004) and used in several works (eg., T06, Lee & Erdogdu 2007, S09). This alternative expression is characterized by a parameter  $c$  and, from the comparison between Equation (9) of S09 and Equation (7) of the

present work, it is possible to obtain the following expression relating both characteristic parameters:

$$p = \sqrt{1 + \frac{3c}{2(1-c)}} \quad (9)$$

### 4.3. Statistical computation of $P(\langle \cos \theta \rangle)$

Different approaches have been used to deal with the indetermination of the values of  $\zeta$ . For example, Kashikawa & Okamura (1992) uses the two values of  $\zeta$  independently. Another possibility is to use just one sign in the definition of  $\zeta$  as done by Lee & Erdogdu (2007). However, these authors acknowledge that this decreases the strength of the measured alignment.

On the other hand, T06 and S09 have overcome the problem with the indetermination of the values of  $\zeta$  using only edge-on and face-on galaxies, for which the direction of the spin is well determined. The main disadvantage of this approach is that the number of galaxies suitable for computing  $P(\langle \cos \theta \rangle)$  is greatly reduced. For example, using the criteria from T06, the fraction of galaxies that can be used is  $\sim 22\%$  of all the disk galaxies.

We opted for a statistical approach that allows to compute a corrected distribution  $P_c(\langle \cos \theta \rangle)$  from the combination of the distributions  $P(\langle \cos \theta \rangle)$  obtained using both signs.

In Appendix A we describe in detail this procedure. We also show in this appendix the results from several Monte Carlo simulations that show the ability of the procedure to recover the correct values of  $p$  (Table 7).

The fact that we actually do not know the real values of  $\zeta$  is reflected in the uncertainties of the procedure. Although the values of  $p$  are well recovered, the uncertainties measured from the simulations are larger than those expected from considering just the size of the sample,  $N_g$ . Of course, this is because we are not using the real values of  $\zeta$ . Nevertheless, from the simulations we have obtained that our procedure has a predictability power equivalent to that of a sample  $0.6 N_g$  with complete knowledge of the real values of  $\zeta$ . Let's remember that the common procedure of using only face-on or edge-on galaxies is restricted to  $\sim 20\%$  of the total amount of spiral galaxies. This means that our statistical procedure increases by a factor of 3 the effective number of galaxies with respect to previous works.

## 5. Results

Using the procedure described in Appendix A, we have computed the corrected distribution  $P_c(\langle \cos \theta \rangle)$  of the sample of galaxies around voids. Given the large size of our initial sample, we have also computed  $P_c(\langle \cos \theta \rangle)$  for different subsamples combining different sizes of voids and shells around them.

An important point of our analysis has been to establish the significance of our results in a robust way. This is done by comparing, in each case, the measured signal with the standard deviation  $\sigma_{\langle \cos \theta \rangle}$  of the theoretical distribution in case of null signal, i.e.  $\langle \cos \theta \rangle = 0.5$ .<sup>10</sup> In the situation of complete knowledge of the real values of  $\zeta$ , we would have  $\sigma_{\langle \cos \theta \rangle} = (\sqrt{12 \times N_g})^{-1}$  for a sample of  $N_g$  measures. However, we have already shown that our procedure has uncertainties equivalent to a sample of size  $0.6 N_g$ , therefore, the previous expression needs to be corrected to

$$\sigma_{\langle \cos \theta \rangle} = \frac{1}{\sqrt{12 \times 0.6 \times N_g}}. \quad (10)$$

Knowing the value of  $\sigma_{\langle \cos \theta \rangle}$ , we can establish the signal to noise ratio ( $SNR$ ) of the signal of a subsample of  $N_g$  measurements as:

$$SNR = \frac{0.5 - \langle \cos \theta \rangle_{corr}}{\sigma_{\langle \cos \theta \rangle}}, \quad (11)$$

where  $\langle \cos \theta \rangle_{corr}$  is obtained from the statistical correction and  $\sigma_{\langle \cos \theta \rangle}$  from Equation (10). Note that the denominator is the signal, which corresponds to the difference between the observed value of  $\langle \cos \theta \rangle_{corr}$  and that of the random distribution which is 0.5. For practical reasons, the sign of  $SNR$  has been chosen so that is positive for values of  $p > 1$  ( $\langle \cos \theta \rangle_{corr} < 0.5$ ) and negative for values of  $p < 1$  ( $\langle \cos \theta \rangle_{corr} > 0.5$ ).

In Tables 4 and 5 are shown the main results of our analysis. In Table 4, samples are constructed by setting a minimum value for the radii of the voids ( $R_{Void}^{min}$ ) while, in Table 5, samples are constructed using voids with radii in the ranges  $R_{Void} \pm 0.5 h^{-1} \text{ Mpc}$ .<sup>11</sup> Apart from this difference in the definition of the first column, both tables share the description of the rest of the

<sup>10</sup>In the analysis of the significance is more convenience the use of  $\langle \cos \theta \rangle$  than that of  $p$  because the former has a gaussian distribution but the latter has not.

<sup>11</sup>For convenience, we will refer the samples of the first table as ‘‘cumulative’’ samples and those of the second table as ‘‘differential’’ samples.

columns:  $SW$  is the width of the innermost shell in  $h^{-1}$  Mpc;  $N$  is the number of measures of the sample;  $\langle |\cos \theta| \rangle$  is the mean of the  $|\cos \theta|$ ;  $p$  is the characteristic parameter of Equation (7); and  $SNR$  is the signal to noise ratio computed with Equation (11). From simulations it has been found that results obtained with less than  $\sim 100$  measures are not reliable, therefore, samples with less than this number have been flagged with a question mark beside the value of the  $SNR$ .

Errors in  $\langle |\cos \theta| \rangle$  are computed using the standard deviation of  $|\cos \theta|$  resulting from 10000 Monte Carlo simulations with no signal (see below) corrected using Equations (B1-B3) assuming the following relation:

$$\frac{\sigma_{\langle |\cos \theta| \rangle}(p \neq 1; corr)}{\sigma_{\langle |\cos \theta| \rangle}(p \neq 1; theo)} = \frac{\sigma_{\langle |\cos \theta| \rangle}(p = 1; sim)}{\sigma_{\langle |\cos \theta| \rangle}(p = 1; theo)} \quad (12)$$

where  $\sigma_{\langle |\cos \theta| \rangle}(p; theo)$  is computed using the theoretical expressions described in Equations (B1-B3),  $\sigma_{\langle |\cos \theta| \rangle}(p = 1; sim)$  is computed from the simulations and  $\sigma_{\langle |\cos \theta| \rangle}(p \neq 1; corr)$  is the final value used in Tables 4-5.

Since  $p$  does not follow a Gaussian distribution, for this parameter we provide the confidence levels at  $1\sigma$  again correcting the theoretical values from Equations (B5-B6) with the confidence levels measured from the simulations with no signal.

In Figures 3 and 4 are plotted the values of  $p$  (upper panels) and  $SNR$  (lower panels) as a function of the radius of the voids, for the cumulative and differential samples, respectively. In the first figure the plotted radius is the minimum radius of each sample and in the second the central radius of each bin. In different colors are plotted the 10 shells widths that have been explored.

The first result is that  $p < 1$  for most of the subsamples. This means that the direction of the spin of the galaxies tends to be parallel to the radial direction of the void. Despite of the large sample that we are using and the additional statistical correction, we find that the significance of the signal is not high most of the times and is dependent on the radius of the voids. The highest significance is reached when selecting galaxies around voids, larger than  $16 h^{-1}$  Mpc in shells of  $3 h^{-1}$  Mpc ( $|SNR| > 3.6$ ) using 179 galaxies, but the  $|SNR|$  is higher than 3 increasing the width of the shell up to  $7 h^{-1}$  Mpc and the sample size to 614 galaxies. Therefore, the further the galaxies are from the surface of the void, the lower is the signal although the increase in the size sample keeps the significance high.

The relation between the strength of the alignment and the radius of the void is clearly shown in Figure 4 where the differential samples are used. For voids smaller than  $\sim 15 h^{-1}$  Mpc these results are compatible with a random distribution. It is for voids  $\gtrsim 15 h^{-1}$  Mpc when it appears a signal of alignment, although given the smaller size of the samples the highest significance reached is 2.96 for voids with  $16 h^{-1} \text{ Mpc} \leq R_{Void} \leq 17 h^{-1} \text{ Mpc}$  and a shell of  $6 h^{-1}$  Mpc.

Figure 6 shows the corrected histograms of  $\theta$  values (see Equation A5) for the cases in which is reached the maximum  $SNR$  for the cumulative (left panel) and the differential samples (right panel). The continuous red line shows the analytical model described by Equation (7) with the  $p$  values corresponding to these two maxima.

To compute in a more robust way the significance level of our results we need to compare them with a control sample with no signal. To construct this control sample, we have run 10000 Monte Carlo simulations in which the spin direction of the galaxies (determined by their position angles and axial ratios) has been shuffled so that each galaxy it is assigned the spin direction of any other galaxy randomly selected. This procedure has the advantage of ensuring the randomness of the spin distribution and, therefore, the lack of any alignment signal, while using real data.

For each simulation we have repeated the analysis performed in the real data using cumulative subsamples, and we have also computed 2 statistics used both in the real data and in the simulations. These statistics were computed as follows: for each bin in  $R_{Void}$ , the mean (median) value of the  $SNR$  measured in the 10 different shell widths was computed and the extreme value (i.e. with highest absolute value) of each simulation was kept.

The significance level from each statistic is computed as

$$1 - 2f(\text{extreme}\{SNR_{Sim}\} < \text{extreme}\{SNR_{Real}\}),$$

where  $f(\text{extreme}\{SNR_{Sim}\} < \text{extreme}\{SNR_{Real}\})$  is the fraction of simulations with extreme values of the mean (median) of SNR lower than the observed ones ( $-2.73$  for the mean;  $-3.10$  for the median). The fact of multiplying by two the observed fraction takes into account that we are considering only one side of the distribution of the statistics.

The results from this analysis are summarized in Table 3. Using the mean we obtain a significance of



98.8% which improves slightly to 99.5% if the median is used instead.

Although this test ensures the existence of a global signal, we have also checked that the increase of the  $SNR$  with the radius of the voids shown in Tables 4 and 5 is not just a consequence of the variation in the size of the samples. Figure 5 shows the dependence of the  $SNR$  with the size of the samples ( $N_g$ ). For clarity purposes we have restricted the analysis to the voids larger than  $14 h^{-1}$  Mpc. Each line corresponds to different limits in  $R_{Void}$  and each point corresponds to a shell width. It can be seen that all subsamples show a similar trend with the width of the shell, showing the maximum value of  $SNR$ , in absolute value, at intermediate shell widths. Also, for subsamples with similar sizes, the  $SNR$  shows variations depending on the size of the voids and shells, rejecting the hypothesis that the variations of the  $SNR$  are due only to variations of the size of the samples.

Finally, to check the dependence of the significance of the signal with the distance of the galaxies to the surface of the void, we have constructed subsamples containing galaxies closer than  $5 h^{-1}$  Mpc of the voids' surface and galaxies between  $5 h^{-1}$  Mpc and  $10 h^{-1}$  Mpc. With these two groups of galaxies we have repeated the analysis (only cumulative). In Table 6 are presented the results of this analysis which show that galaxies at distances larger than  $5 h^{-1}$  Mpc do not present any significance alignment.

## 6. Discussion

We have analysed a large sample of galaxies around 699 voids with radius larger than  $10 h^{-1}$  Mpc up to  $z = 0.12$ . We have found that for voids with ra-

Criteria	$N_{Sim}$	%
$\min\{\langle SNR \rangle\} < -2.73$	58	98.8
$\min\{\text{median}(SNR)\} < -3.10$	23	99.5

Table 3: Results from 10000 simulations with reshuffling of position angle and axial ratio between galaxies, showing the number of simulations presenting values for two statistics smaller than the observed values ( $\text{extreme}\{\langle SNR \rangle\}(\text{Real Data}) = -2.73$ ;  $\text{extreme}\{\text{median}(SNR)\}(\text{Real data}) = -3.10$ ). The last column shows the significance of the result, which takes into account that we are considering only one side of the distribution of the statistics. See text for more details.

dus  $\gtrsim 15 h^{-1}$  Mpc and within a shell not larger than  $\sim 5 h^{-1}$  Mpc, disk galaxies present a significant tendency to have their spin vectors aligned with the radial direction of the void.

The maximum  $|SNR| = 3.62$  is measured for voids with  $R_{Void} \geq 16 h^{-1}$  Mpc and a shell width of  $3 h^{-1}$  Mpc with a strength of the alignment  $p = 0.664^{+0.083}_{-0.074}$ . However, this value gives an overestimation of the real strength since has been selected as the best case out of many subsamples.

In the next sections we compare our results with previous empirical works and with results from numerical simulations.

### 6.1. Comparison with empirical works

From the observational point of view, T06 and, more recently, S09 have performed a similar analysis to the one done here. T06 analysed 201 face-on and edge-on galaxies around voids with  $R > 10 h^{-1}$  Mpc using data from the SDSS-DR3 and the 2dFRGS. They found a significant tendency of the spin of the galaxies to be in the direction perpendicular to the radial direction of the void. More recently, S09 using two samples of 578 and 258 galaxies from the SDSS-DR6 with similar selection criteria found no statistical evidence for departure from random orientations.

Using the same criteria on the size of the voids ( $R_{Void} > 10 h^{-1}$  Mpc) and on the width of the shell ( $4 h^{-1}$  Mpc) as in those previous works, we find no significance alignment ( $p = 0.998$ ;  $SNR = -0.15$ ; see Table 4). The size of the sample used to establish this result is of 11060 galaxies, which after applying the correction factor of 0.6, means an equivalent size of 6636 galaxies. This number is 8 times larger the size used by S09.

For a better comparison, we have computed the signal of the alignment using criteria similar to that of S09 regarding the selection of spiral galaxies ( $g - r < 0.6$ ) and the definition of edge-on ( $b/a < 0.27$ ) and face-on ( $b/a < 0.96$ ) galaxies<sup>12</sup>. However, we keep our limit in  $M_r$  instead of using  $M_r > -21 + 5 \log h$  as done by S09 because otherwise the final number of galaxies would be too small. After applying these criteria, we finished with a sample of 252 face-on and edge-on spiral galaxies. The value of  $p$  obtained with this sample is 0.993 with a  $SNR = 0.1$  and, therefore, compatible

<sup>12</sup>We used a slightly different way to compute the axial ratio  $b/a$  compared with S09, however, we do not consider this to have a significance effect on our comparison.

$R_{Void}^{min}$	$SW$	$N$	$\langle \cos \theta \rangle$	$p$	SNR	$R_{Void}^{min}$	$SW$	$N$	$\langle \cos \theta \rangle$	$p$	SNR
10	1	2320	0.501 ± 0.009	0.995 <sup>+0.032</sup> <sub>-0.033</sub>	-0.157	10	6	20068	0.501 ± 0.003	0.998 <sup>+0.012</sup> <sub>-0.013</sub>	-0.193
11	1	1497	0.499 ± 0.011	1.004 <sup>+0.043</sup> <sub>-0.044</sub>	0.106	11	6	12997	0.502 ± 0.003	0.990 <sup>+0.013</sup> <sub>-0.014</sub>	-0.750
12	1	884	0.497 ± 0.014	1.011 <sup>+0.054</sup> <sub>-0.055</sub>	0.211	12	6	7777	0.506 ± 0.004	0.977 <sup>+0.017</sup> <sub>-0.018</sub>	-1.355
13	1	503	0.500 ± 0.019	0.998 <sup>+0.052</sup> <sub>-0.053</sub>	-0.026	13	6	4538	0.504 ± 0.007	0.985 <sup>+0.025</sup> <sub>-0.026</sub>	-0.702
14	1	243	0.506 ± 0.026	0.975 <sup>+0.073</sup> <sub>-0.074</sub>	-0.260	14	6	2283	0.510 ± 0.009	0.962 <sup>+0.032</sup> <sub>-0.033</sub>	-1.256
15	1	128	0.511 ± 0.034	0.956 <sup>+0.114</sup> <sub>-0.115</sub>	-0.341	15	6	1173	0.530 ± 0.011	0.887 <sup>+0.040</sup> <sub>-0.041</sub>	-2.746
16	1	48	0.551 ± 0.057	0.815 <sup>+0.180</sup> <sub>-0.181</sub>	-0.948 ?	16	6	488	0.556 ± 0.018	0.798 <sup>+0.057</sup> <sub>-0.058</sub>	-3.332
17	1	24	0.572 ± 0.085	0.747 <sup>+0.185</sup> <sub>-0.186</sub>	-0.951 ?	17	6	274	0.539 ± 0.024	0.856 <sup>+0.082</sup> <sub>-0.083</sub>	-1.727
18	1	12	0.475 ± 0.145	1.105 <sup>+0.229</sup> <sub>-0.230</sub>	0.232 ?	18	6	129	0.536 ± 0.038	0.866 <sup>+0.134</sup> <sub>-0.135</sub>	-1.094
10	2	4683	0.504 ± 0.005	0.985 <sup>+0.024</sup> <sub>-0.025</sub>	-0.687	10	7	25473	0.501 ± 0.002	0.996 <sup>+0.010</sup> <sub>-0.011</sub>	-0.436
11	2	2998	0.502 ± 0.008	0.990 <sup>+0.031</sup> <sub>-0.032</sub>	-0.355	11	7	16489	0.504 ± 0.003	0.986 <sup>+0.013</sup> <sub>-0.014</sub>	-1.249
12	2	1781	0.509 ± 0.010	0.964 <sup>+0.037</sup> <sub>-0.038</sub>	-1.032	12	7	9807	0.507 ± 0.004	0.971 <sup>+0.016</sup> <sub>-0.017</sub>	-1.925
13	2	1015	0.514 ± 0.013	0.945 <sup>+0.049</sup> <sub>-0.050</sub>	-1.220	13	7	5740	0.505 ± 0.006	0.980 <sup>+0.021</sup> <sub>-0.022</sub>	-1.016
14	2	498	0.528 ± 0.018	0.892 <sup>+0.067</sup> <sub>-0.068</sub>	-1.705	14	7	2878	0.511 ± 0.008	0.958 <sup>+0.029</sup> <sub>-0.030</sub>	-1.534
15	2	262	0.552 ± 0.024	0.812 <sup>+0.087</sup> <sub>-0.088</sub>	-2.252	15	7	1471	0.526 ± 0.010	0.903 <sup>+0.038</sup> <sub>-0.039</sub>	-2.628
16	2	109	0.611 ± 0.036	0.637 <sup>+0.086</sup> <sub>-0.087</sub>	-3.106	16	7	614	0.547 ± 0.016	0.830 <sup>+0.054</sup> <sub>-0.055</sub>	-3.092
17	2	61	0.627 ± 0.050	0.596 <sup>+0.121</sup> <sub>-0.122</sub>	-2.653 ?	17	7	339	0.534 ± 0.021	0.872 <sup>+0.076</sup> <sub>-0.077</sub>	-1.684
18	2	25	0.554 ± 0.117	0.805 <sup>+0.138</sup> <sub>-0.139</sub>	-0.725 ?	18	7	161	0.529 ± 0.035	0.889 <sup>+0.125</sup> <sub>-0.126</sub>	-1.002
10	3	7592	0.501 ± 0.004	0.997 <sup>+0.018</sup> <sub>-0.019</sub>	-0.185	10	8	31560	0.500 ± 0.002	0.998 <sup>+0.010</sup> <sub>-0.011</sub>	-0.192
11	3	4877	0.504 ± 0.006	0.983 <sup>+0.023</sup> <sub>-0.024</sub>	-0.827	11	8	20428	0.503 ± 0.003	0.990 <sup>+0.011</sup> <sub>-0.012</sub>	-0.991
12	3	2888	0.512 ± 0.008	0.953 <sup>+0.030</sup> <sub>-0.031</sub>	-1.751	12	8	12239	0.505 ± 0.003	0.979 <sup>+0.013</sup> <sub>-0.014</sub>	-1.565
13	3	1663	0.518 ± 0.010	0.930 <sup>+0.038</sup> <sub>-0.039</sub>	-1.979	13	8	7129	0.505 ± 0.004	0.981 <sup>+0.016</sup> <sub>-0.017</sub>	-1.074
14	3	826	0.535 ± 0.014	0.869 <sup>+0.048</sup> <sub>-0.049</sub>	-2.703	14	8	3609	0.508 ± 0.007	0.969 <sup>+0.028</sup> <sub>-0.029</sub>	-1.260
15	3	429	0.551 ± 0.019	0.816 <sup>+0.068</sup> <sub>-0.069</sub>	-2.819	15	8	1833	0.519 ± 0.009	0.928 <sup>+0.034</sup> <sub>-0.035</sub>	-2.157
16	3	179	0.601 ± 0.029	0.664 <sup>+0.081</sup> <sub>-0.082</sub>	-3.620	16	8	756	0.533 ± 0.015	0.875 <sup>+0.051</sup> <sub>-0.052</sub>	-2.468
17	3	102	0.601 ± 0.040	0.663 <sup>+0.112</sup> <sub>-0.113</sub>	-2.747	17	8	423	0.521 ± 0.019	0.918 <sup>+0.071</sup> <sub>-0.072</sub>	-1.180
18	3	45	0.574 ± 0.087	0.742 <sup>+0.115</sup> <sub>-0.116</sub>	-1.331 ?	18	8	203	0.505 ± 0.030	0.978 <sup>+0.120</sup> <sub>-0.121</sub>	-0.209
10	4	11060	0.501 ± 0.005	0.998 <sup>+0.015</sup> <sub>-0.016</sub>	-0.148	10	9	38273	0.503 ± 0.002	0.989 <sup>+0.009</sup> <sub>-0.010</sub>	-1.500
11	4	7083	0.502 ± 0.005	0.991 <sup>+0.016</sup> <sub>-0.017</sub>	-0.521	11	9	24848	0.502 ± 0.002	0.991 <sup>+0.010</sup> <sub>-0.011</sub>	-0.991
12	4	4232	0.507 ± 0.007	0.974 <sup>+0.024</sup> <sub>-0.025</sub>	-1.137	12	9	14941	0.505 ± 0.003	0.981 <sup>+0.014</sup> <sub>-0.015</sub>	-1.599
13	4	2463	0.509 ± 0.009	0.963 <sup>+0.031</sup> <sub>-0.032</sub>	-1.265	13	9	8684	0.504 ± 0.004	0.984 <sup>+0.016</sup> <sub>-0.017</sub>	-1.038
14	4	1229	0.532 ± 0.012	0.881 <sup>+0.041</sup> <sub>-0.042</sub>	-2.974	14	9	4368	0.510 ± 0.007	0.961 <sup>+0.024</sup> <sub>-0.025</sub>	-1.747
15	4	632	0.545 ± 0.016	0.836 <sup>+0.044</sup> <sub>-0.045</sub>	-3.021	15	9	2203	0.519 ± 0.009	0.927 <sup>+0.031</sup> <sub>-0.032</sub>	-2.373
16	4	256	0.581 ± 0.025	0.722 <sup>+0.075</sup> <sub>-0.076</sub>	-3.459	16	9	904	0.522 ± 0.013	0.917 <sup>+0.030</sup> <sub>-0.031</sub>	-1.736
17	4	148	0.566 ± 0.034	0.768 <sup>+0.103</sup> <sub>-0.104</sub>	-2.141	17	9	519	0.511 ± 0.017	0.955 <sup>+0.068</sup> <sub>-0.069</sub>	-0.703
18	4	70	0.527 ± 0.060	0.898 <sup>+0.184</sup> <sub>-0.185</sub>	-0.603 ?	18	9	247	0.493 ± 0.028	1.028 <sup>+0.111</sup> <sub>-0.112</sub>	0.287
10	5	15289	0.500 ± 0.003	0.999 <sup>+0.013</sup> <sub>-0.014</sub>	-0.053	10	10	45522	0.502 ± 0.002	0.991 <sup>+0.009</sup> <sub>-0.010</sub>	-1.260
11	5	9845	0.505 ± 0.004	0.980 <sup>+0.017</sup> <sub>-0.018</sub>	-1.365	11	10	29653	0.502 ± 0.002	0.994 <sup>+0.010</sup> <sub>-0.011</sub>	-0.703
12	5	5865	0.509 ± 0.006	0.964 <sup>+0.021</sup> <sub>-0.022</sub>	-1.864	12	10	17929	0.505 ± 0.003	0.981 <sup>+0.012</sup> <sub>-0.013</sub>	-1.723
13	5	3431	0.509 ± 0.007	0.963 <sup>+0.029</sup> <sub>-0.030</sub>	-1.492	13	10	10406	0.504 ± 0.004	0.983 <sup>+0.013</sup> <sub>-0.014</sub>	-1.195
14	5	1712	0.525 ± 0.010	0.904 <sup>+0.035</sup> <sub>-0.036</sub>	-2.814	14	10	5226	0.510 ± 0.006	0.961 <sup>+0.022</sup> <sub>-0.023</sub>	-1.938
15	5	879	0.541 ± 0.013	0.847 <sup>+0.045</sup> <sub>-0.046</sub>	-3.297	15	10	2585	0.517 ± 0.007	0.935 <sup>+0.026</sup> <sub>-0.027</sub>	-2.305
16	5	355	0.569 ± 0.021	0.758 <sup>+0.065</sup> <sub>-0.066</sub>	-3.473	16	10	1078	0.523 ± 0.012	0.911 <sup>+0.035</sup> <sub>-0.036</sub>	-2.054
17	5	201	0.556 ± 0.029	0.798 <sup>+0.080</sup> <sub>-0.081</sub>	-2.141	17	10	624	0.516 ± 0.016	0.939 <sup>+0.061</sup> <sub>-0.062</sub>	-1.062
18	5	95	0.520 ± 0.048	0.924 <sup>+0.166</sup> <sub>-0.167</sub>	-0.516 ?	18	10	284	0.509 ± 0.025	0.963 <sup>+0.059</sup> <sub>-0.060</sub>	-0.425

Table 4: Statistics for subsamples with different sizes of voids and shells. This table corresponds to the “cumulative samples” in which each sample contains galaxies around voids with radius larger than  $R_{Void}^{min}$ .  $R_{Void}^{min}$ : Lower limit of the void’s radius in each sample, in  $h^{-1}$  Mpc.  $SW$ : Width of the shell, in  $h^{-1}$  Mpc.  $\langle \cos \theta \rangle$ : Average of the distribution of  $\langle \cos \theta \rangle$ .  $p$ : Resulting value of the  $p$  parameter of Equation (7).  $S/NR$ : Theoretical signal to noise ratio computed with Equation (11). Samples with less than 100 galaxies have been flagged with a question mark nearby the  $S/NR$  to remark the low reliability of these results. Errors in  $\langle \cos \theta \rangle$  and  $p$  are computed using formulae in Appendix B in combination with Monte Carlo simulations. See text for more details.

$R_{Void}$	$S.W$	$N$	$\langle \cos \theta \rangle$	$p$	$SNR$	$R_{Void}$	$S.W$	$N$	$ \cos \theta $	$p$	$SNR$
10.5	1	823	0.509 ± 0.014	0.966 <sup>+0.055</sup> <sub>-0.053</sub>	-0.657	10.5	6	7071	0.497 ± 0.004	1.014 <sup>+0.020</sup> <sub>-0.020</sub>	0.774
11.5	1	613	0.500 ± 0.017	1.001 <sup>+0.088</sup> <sub>-0.085</sub>	0.022	11.5	6	5220	0.500 ± 0.006	1.000 <sup>+0.024</sup> <sub>-0.024</sub>	-0.013
12.5	1	381	0.497 ± 0.020	1.014 <sup>+0.089</sup> <sub>-0.084</sub>	0.179	12.5	6	3239	0.510 ± 0.008	0.961 <sup>+0.023</sup> <sub>-0.023</sub>	-1.509
13.5	1	260	0.492 ± 0.025	1.031 <sup>+0.107</sup> <sub>-0.102</sub>	0.330	13.5	6	2255	0.496 ± 0.009	1.018 <sup>+0.036</sup> <sub>-0.036</sub>	0.555
14.5	1	115	0.503 ± 0.038	0.987 <sup>+0.192</sup> <sub>-0.182</sub>	-0.092	14.5	6	1110	0.489 ± 0.013	1.046 <sup>+0.035</sup> <sub>-0.035</sub>	1.006
15.5	1	80	0.482 ± 0.044	1.076 <sup>+0.183</sup> <sub>-0.195</sub>	0.441 ?	15.5	6	685	0.509 ± 0.015	0.964 <sup>+0.059</sup> <sub>-0.059</sub>	-0.645
16.5	1	24	0.528 ± 0.080	0.893 <sup>+0.236</sup> <sub>-0.238</sub>	-0.372 ?	16.5	6	214	0.575 ± 0.027	0.738 <sup>+0.082</sup> <sub>-0.082</sub>	-2.960
17.5	1	12	0.636 ± 0.104	0.572 <sup>+0.198</sup> <sub>-0.198</sub>	-1.264 ?	17.5	6	145	0.542 ± 0.031	0.845 <sup>+0.105</sup> <sub>-0.105</sub>	-1.354
18.5	1	12	0.475 ± 0.145	1.105 <sup>+0.315</sup> <sub>-0.315</sub>	0.232 ?	18.5	6	129	0.536 ± 0.038	0.866 <sup>+0.131</sup> <sub>-0.131</sub>	-1.094
10.5	2	1685	0.501 ± 0.010	0.996 <sup>+0.059</sup> <sub>-0.059</sub>	-0.114	10.5	7	8984	0.496 ± 0.004	1.017 <sup>+0.018</sup> <sub>-0.018</sub>	1.044
11.5	2	1217	0.497 ± 0.012	1.011 <sup>+0.049</sup> <sub>-0.049</sub>	0.265	11.5	7	6682	0.501 ± 0.006	0.997 <sup>+0.026</sup> <sub>-0.026</sub>	-0.178
12.5	2	766	0.502 ± 0.014	0.990 <sup>+0.058</sup> <sub>-0.058</sub>	-0.181	12.5	7	4067	0.512 ± 0.007	0.953 <sup>+0.022</sup> <sub>-0.022</sub>	-2.051
13.5	2	517	0.501 ± 0.018	0.996 <sup>+0.073</sup> <sub>-0.073</sub>	-0.055	13.5	7	2862	0.497 ± 0.008	1.012 <sup>+0.033</sup> <sub>-0.033</sub>	0.434
14.5	2	236	0.498 ± 0.027	1.009 <sup>+0.114</sup> <sub>-0.114</sub>	0.092	14.5	7	1407	0.494 ± 0.011	1.023 <sup>+0.046</sup> <sub>-0.046</sub>	0.560
15.5	2	153	0.504 ± 0.032	0.986 <sup>+0.152</sup> <sub>-0.152</sub>	-0.121	15.5	7	857	0.511 ± 0.014	0.957 <sup>+0.042</sup> <sub>-0.042</sub>	-0.859
16.5	2	48	0.587 ± 0.054	0.702 <sup>+0.131</sup> <sub>-0.131</sub>	-1.627 ?	16.5	7	275	0.562 ± 0.025	0.779 <sup>+0.058</sup> <sub>-0.058</sub>	-2.763
17.5	2	36	0.664 ± 0.057	0.506 <sup>+0.124</sup> <sub>-0.124</sub>	-2.638 ?	17.5	7	178	0.538 ± 0.028	0.859 <sup>+0.096</sup> <sub>-0.096</sub>	-1.356
18.5	2	25	0.554 ± 0.118	0.805 <sup>+0.333</sup> <sub>-0.333</sub>	-0.725 ?	18.5	7	161	0.529 ± 0.034	0.889 <sup>+0.112</sup> <sub>-0.112</sub>	-1.002
10.5	3	2715	0.494 ± 0.008	1.025 <sup>+0.031</sup> <sub>-0.031</sub>	0.851	10.5	8	11132	0.499 ± 0.004	1.006 <sup>+0.015</sup> <sub>-0.015</sub>	0.421
11.5	3	1989	0.495 ± 0.009	1.019 <sup>+0.036</sup> <sub>-0.036</sub>	0.550	11.5	8	8189	0.499 ± 0.005	1.006 <sup>+0.019</sup> <sub>-0.019</sub>	0.348
12.5	3	1225	0.506 ± 0.012	0.978 <sup>+0.038</sup> <sub>-0.038</sub>	-0.532	12.5	8	5110	0.506 ± 0.005	0.976 <sup>+0.029</sup> <sub>-0.029</sub>	-1.153
13.5	3	837	0.500 ± 0.014	1.002 <sup>+0.057</sup> <sub>-0.057</sub>	0.030	13.5	8	3520	0.501 ± 0.007	0.995 <sup>+0.038</sup> <sub>-0.038</sub>	-0.202
14.5	3	397	0.517 ± 0.021	0.935 <sup>+0.076</sup> <sub>-0.076</sub>	-0.902	14.5	8	1776	0.497 ± 0.010	1.011 <sup>+0.028</sup> <sub>-0.028</sub>	0.314
15.5	3	250	0.511 ± 0.026	0.955 <sup>+0.077</sup> <sub>-0.077</sub>	-0.485	15.5	8	1077	0.508 ± 0.012	0.970 <sup>+0.049</sup> <sub>-0.049</sub>	-0.674
16.5	3	77	0.597 ± 0.042	0.676 <sup>+0.116</sup> <sub>-0.116</sub>	-2.278 ?	16.5	8	333	0.549 ± 0.023	0.820 <sup>+0.075</sup> <sub>-0.075</sub>	-2.417
17.5	3	57	0.620 ± 0.047	0.613 <sup>+0.126</sup> <sub>-0.126</sub>	-2.427 ?	17.5	8	220	0.533 ± 0.025	0.877 <sup>+0.087</sup> <sub>-0.087</sub>	-1.300
18.5	3	45	0.574 ± 0.084	0.742 <sup>+0.135</sup> <sub>-0.135</sub>	-1.331 ?	18.5	8	203	0.505 ± 0.030	0.978 <sup>+0.116</sup> <sub>-0.116</sub>	-0.209
10.5	4	3977	0.494 ± 0.006	1.023 <sup>+0.026</sup> <sub>-0.026</sub>	0.951	10.5	9	13425	0.499 ± 0.003	1.005 <sup>+0.015</sup> <sub>-0.015</sub>	0.378
11.5	4	2851	0.497 ± 0.008	1.011 <sup>+0.031</sup> <sub>-0.031</sub>	0.377	11.5	9	9907	0.499 ± 0.004	1.006 <sup>+0.016</sup> <sub>-0.016</sub>	0.394
12.5	4	1769	0.503 ± 0.010	0.988 <sup>+0.033</sup> <sub>-0.033</sub>	-0.349	12.5	9	6257	0.508 ± 0.006	0.967 <sup>+0.018</sup> <sub>-0.018</sub>	-1.795
13.5	4	1234	0.485 ± 0.012	1.063 <sup>+0.050</sup> <sub>-0.050</sub>	1.440	13.5	9	4316	0.499 ± 0.007	1.006 <sup>+0.025</sup> <sub>-0.025</sub>	0.250
14.5	4	597	0.515 ± 0.017	0.943 <sup>+0.064</sup> <sub>-0.064</sub>	-0.965	14.5	9	2165	0.498 ± 0.009	1.008 <sup>+0.039</sup> <sub>-0.039</sub>	0.243
15.5	4	376	0.518 ± 0.020	0.929 <sup>+0.065</sup> <sub>-0.065</sub>	-0.962	15.5	9	1299	0.519 ± 0.011	0.927 <sup>+0.037</sup> <sub>-0.037</sub>	-1.840
16.5	4	108	0.596 ± 0.037	0.678 <sup>+0.104</sup> <sub>-0.104</sub>	-2.671	16.5	9	385	0.533 ± 0.021	0.877 <sup>+0.074</sup> <sub>-0.074</sub>	-1.720
17.5	4	78	0.594 ± 0.041	0.682 <sup>+0.116</sup> <sub>-0.116</sub>	-2.239 ?	17.5	9	272	0.525 ± 0.024	0.904 <sup>+0.083</sup> <sub>-0.083</sub>	-1.120
18.5	4	70	0.527 ± 0.059	0.898 <sup>+0.130</sup> <sub>-0.130</sub>	-0.603 ?	18.5	9	247	0.493 ± 0.027	1.028 <sup>+0.087</sup> <sub>-0.087</sub>	0.287
10.5	5	5444	0.495 ± 0.006	1.019 <sup>+0.024</sup> <sub>-0.024</sub>	0.919	10.5	10	15869	0.503 ± 0.003	0.986 <sup>+0.013</sup> <sub>-0.013</sub>	-1.173
11.5	5	3980	0.497 ± 0.007	1.013 <sup>+0.024</sup> <sub>-0.024</sub>	0.536	11.5	10	11724	0.497 ± 0.003	1.014 <sup>+0.016</sup> <sub>-0.016</sub>	1.013
12.5	5	2434	0.506 ± 0.009	0.977 <sup>+0.032</sup> <sub>-0.032</sub>	-0.782	12.5	10	7523	0.508 ± 0.004	0.969 <sup>+0.016</sup> <sub>-0.016</sub>	-1.852
13.5	5	1719	0.491 ± 0.010	1.038 <sup>+0.037</sup> <sub>-0.037</sub>	1.041	13.5	10	5180	0.499 ± 0.006	1.005 <sup>+0.023</sup> <sub>-0.023</sub>	0.220
14.5	5	833	0.507 ± 0.015	0.974 <sup>+0.057</sup> <sub>-0.057</sub>	-0.515	14.5	10	2641	0.503 ± 0.008	0.988 <sup>+0.033</sup> <sub>-0.033</sub>	-0.424
15.5	5	524	0.520 ± 0.017	0.922 <sup>+0.068</sup> <sub>-0.068</sub>	-1.238	15.5	10	1507	0.513 ± 0.011	0.950 <sup>+0.034</sup> <sub>-0.034</sub>	-1.324
16.5	5	154	0.583 ± 0.032	0.716 <sup>+0.084</sup> <sub>-0.084</sub>	-2.752	16.5	10	454	0.536 ± 0.020	0.867 <sup>+0.067</sup> <sub>-0.067</sub>	-2.035
17.5	5	106	0.581 ± 0.035	0.720 <sup>+0.106</sup> <sub>-0.106</sub>	-2.249	17.5	10	340	0.521 ± 0.021	0.921 <sup>+0.078</sup> <sub>-0.078</sub>	-1.023
18.5	5	95	0.520 ± 0.047	0.924 <sup>+0.171</sup> <sub>-0.171</sub>	-0.516 ?	18.5	10	284	0.509 ± 0.025	0.963 <sup>+0.094</sup> <sub>-0.094</sub>	-0.425

Table 5: Statistics for subsamples with different size of voids and shells. This table corresponds to the “differential samples” in which each sample contains galaxies around voids with radii in the intervals ( $R_{Void} - 0.5, R_{Void} + 0.5$ ).  $R_{Void}$ : Midpoint of each interval, in  $h^{-1}$  Mpc.  $S.W$ : Width of the shell, in  $h^{-1}$  Mpc.  $\langle \cos \theta \rangle$ : Average of the distribution of  $\langle \cos \theta \rangle$ .  $p$ : Resulting value of the  $p$  parameter of Equation (7).  $S.N.R$ : Theoretical signal to noise ratio computed with Equation (11). Samples with less than 100 galaxies have been flagged with a question mark nearby the  $S.N.R$  to remark the low reliability of these results. Errors in  $\langle \cos \theta \rangle$  and  $p$  are computed using formulae in Appendix B in combination with Monte Carlo simulations. See text for more details.

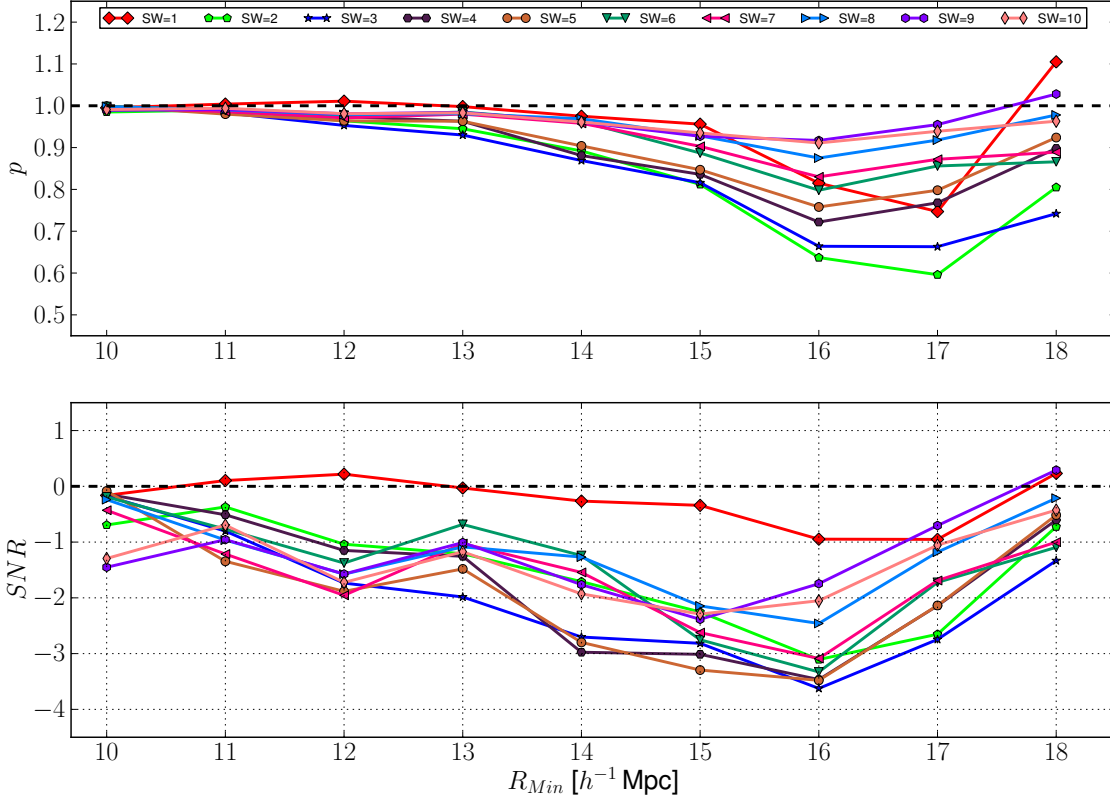


Fig. 3.— *Upper panel:* Values of the parameter  $p$  for subsamples of galaxies in shells of width  $SW$  and voids with radius larger than  $R_{Min}$ . *Lower panel:* Signal to noise of the alignment found for each subsample. This gives the significance of rejecting the null hypothesis of not existence of any alignment.

$R_{Void}^{Min}$	$0 h^{-1} \text{ Mpc} < R_{Shell} \leq 5 h^{-1} \text{ Mpc}$				$5 h^{-1} \text{ Mpc} < R_{Shell} \leq 10 h^{-1} \text{ Mpc}$			
	$N$	$\langle  \cos \theta  \rangle$	$p$	SNR	$N$	$\langle  \cos \theta  \rangle$	$p$	SNR
10	15289	$0.500 \pm 0.003$	$0.999^{+0.012}_{-0.012}$	-0.053	30233	$0.502 \pm 0.002$	$0.992^{+0.009}_{-0.008}$	-0.915
11	9845	$0.505 \pm 0.004$	$0.980^{+0.015}_{-0.015}$	-1.365	19808	$0.501 \pm 0.003$	$0.996^{+0.011}_{-0.010}$	-0.374
12	5865	$0.509 \pm 0.005$	$0.964^{+0.019}_{-0.018}$	-1.864	12064	$0.504 \pm 0.003$	$0.984^{+0.014}_{-0.013}$	-1.170
13	3431	$0.509 \pm 0.006$	$0.963^{+0.025}_{-0.025}$	-1.492	6975	$0.503 \pm 0.004$	$0.988^{+0.017}_{-0.018}$	-0.698
14	1712	$0.525 \pm 0.009$	$0.904^{+0.033}_{-0.033}$	-2.814	3514	$0.502 \pm 0.006$	$0.992^{+0.026}_{-0.024}$	-0.304
15	879	$0.541 \pm 0.013$	$0.847^{+0.044}_{-0.043}$	-3.297	1706	$0.504 \pm 0.009$	$0.985^{+0.036}_{-0.035}$	-0.428
16	355	$0.569 \pm 0.020$	$0.758^{+0.065}_{-0.060}$	-3.473	723	$0.495 \pm 0.014$	$1.020^{+0.058}_{-0.055}$	0.350
17	201	$0.556 \pm 0.027$	$0.798^{+0.090}_{-0.083}$	-2.141	423	$0.491 \pm 0.018$	$1.037^{+0.077}_{-0.073}$	0.496
18	95	$0.520 \pm 0.039$	$0.924^{+0.154}_{-0.133}$	-0.516	189	$0.502 \pm 0.027$	$0.991^{+0.114}_{-0.102}$	-0.080

Table 6: Strength of the alignment for galaxies within a shell up to  $5 h^{-1} \text{ Mpc}$  (left) and for galaxies within a shell between  $5 h^{-1} \text{ Mpc}$  and  $10 h^{-1} \text{ Mpc}$  (right). Each line corresponds to samples of  $N$  galaxies around voids with radius larger than  $R_{Void}^{Min}$ . Errors are computed using theoretical expressions in Appendix B.

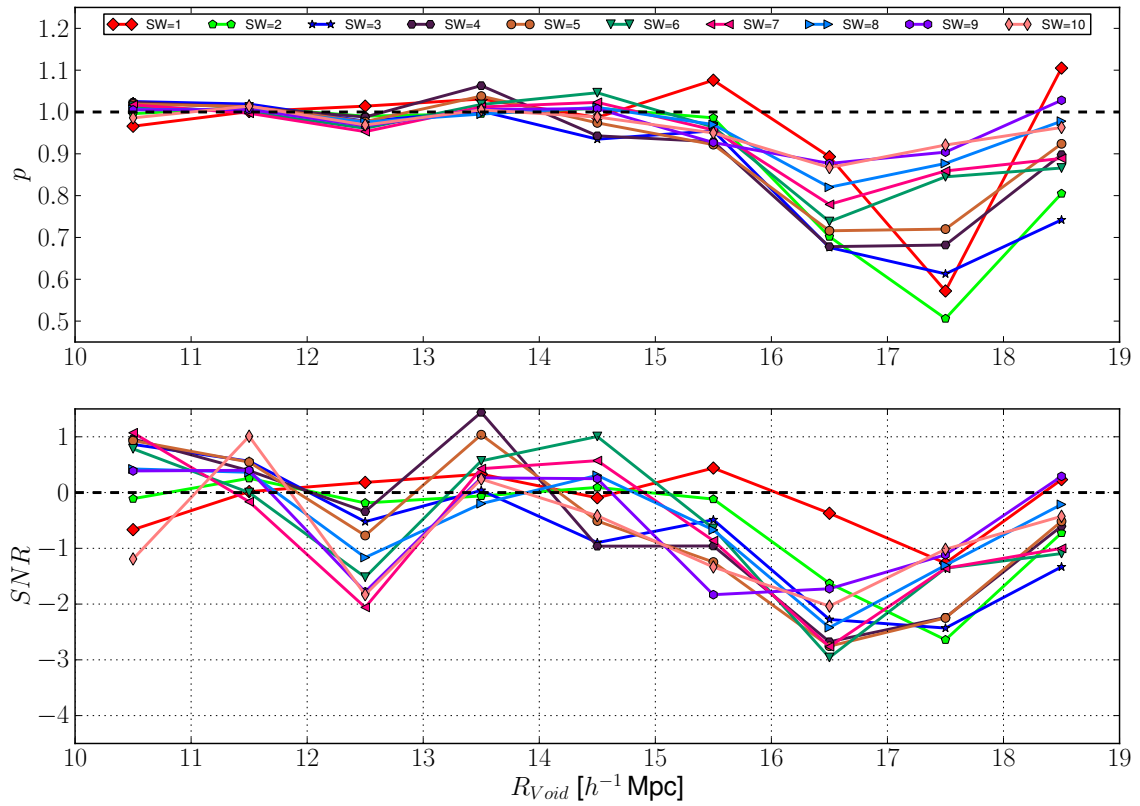


Fig. 4.— *Upper panel:* Values of the parameter  $p$  for subsamples of galaxies in shells of different widths  $SW$  (in  $h^{-1} \text{ Mpc}$ ) and voids in bins of  $1 h^{-1} \text{ Mpc}$  in radius. *Lower panel:* Signal to noise of the alignment found for each subsample. This gives the significance of rejecting the null hypothesis of not existence of any alignment.

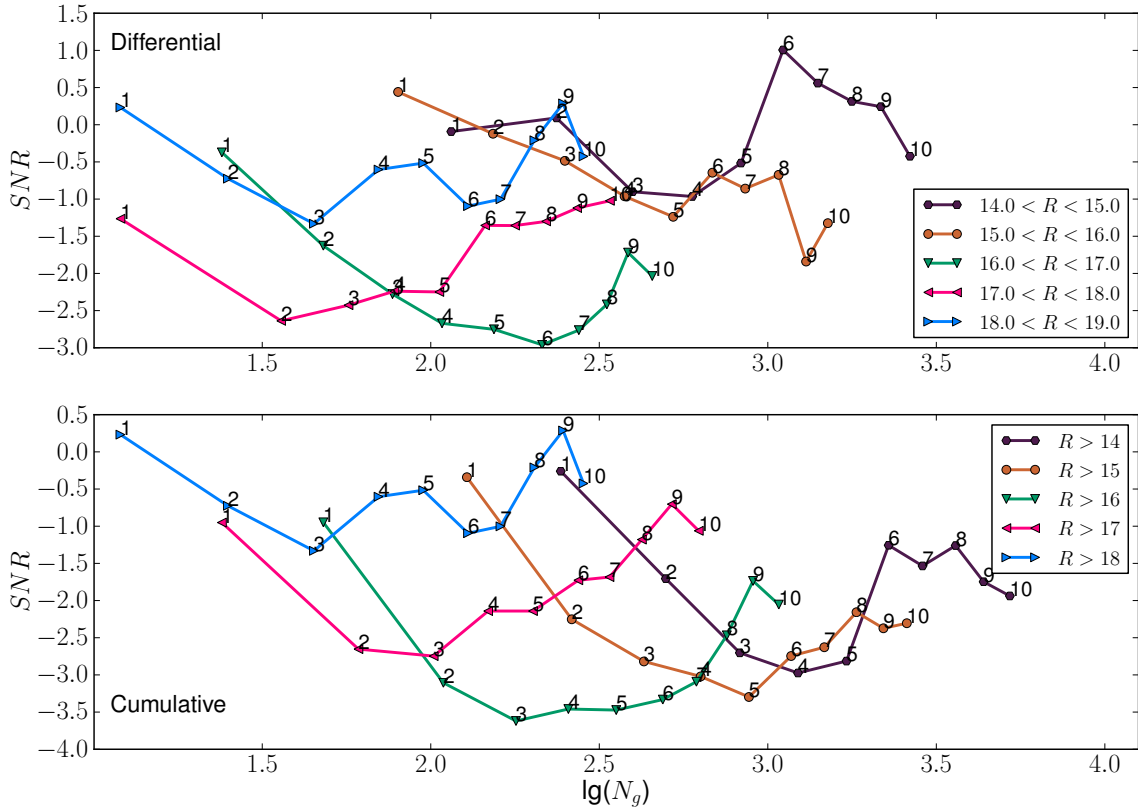


Fig. 5.— Variation of the SNR as a function of the number of galaxies  $N_g$  for different samples. Each line corresponds to a selection in void's radius (differential in the upper panel and cumulative in the lower one) and each number indicates the width of the shell in  $h^{-1}$  Mpc. For practical purposes, only the samples of voids larger than  $14 h^{-1}$  Mpc are shown.

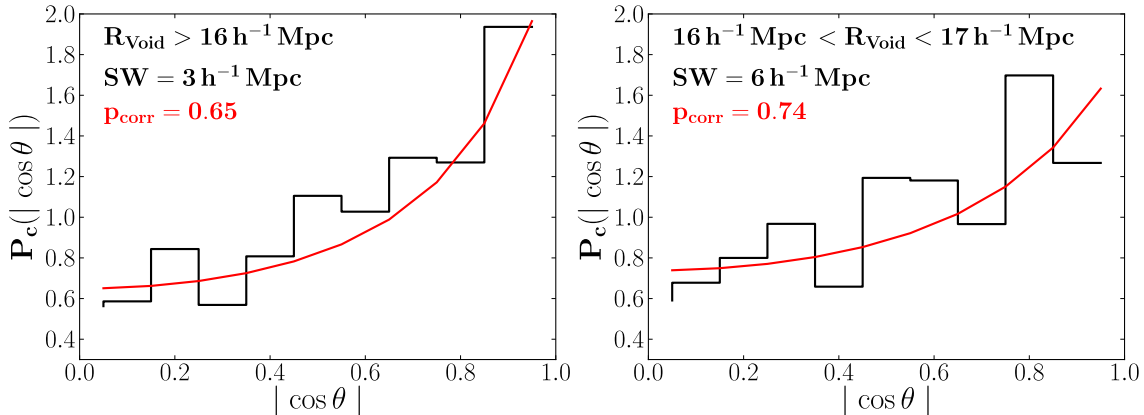


Fig. 6.— Distribution of  $|\cos \theta|$  after applying the statistical correction for the two subsamples that reach the highest  $|SNR|$  in Table 4 (left) and Table 5 (right). The continuous line corresponds to the theoretical model described by Equation (7) for the measured value of  $p$ , shown in the upper left corners.

with a random distribution.

In relation to T06, it is important to note that in that work, the signal presented corresponds to the peak of the signal found after exploring in shells of different widths. Consequently, to properly address the significance of the signal in T06 we have reviewed the data used in that paper taking into account this exploration. To do this, we have run simulations with similar number of galaxies around similar voids ( $R > 10 h^{-1} \text{ Mpc}$ ) searching for the maximum of the  $|SNR|$  in shells of width from  $3 h^{-1} \text{ Mpc}$  to  $7 h^{-1} \text{ Mpc}$  in steps of  $0.1 h^{-1} \text{ Mpc}$ . Then, it has been computed the fraction of simulations with  $\max(|SNR|)$  larger than the one found in T06 when only SDSS data was used ( $\max(SNR_{T06,SDSS}) = 2$ )<sup>13</sup>. After doing our analysis we found that  $\sim 16\%$  of the simulations showed  $\max(|SNR|) > 2$ , decreasing the significance of the result of T06 to  $\sim 84\%$ .

Another observational work on alignment of galaxies with respect to the local large scale structure is that by Lee & Erdogdu (2007). In this paper, the authors computed the shear tidal tensor in the position of each galaxy and measured the angle between each of the principal axes and the spin direction of the galaxy. They found a significant alignment ( $> 6\sigma$ ) between the direction of the spin and the intermediate principal axis of the shear tidal tensor.<sup>14</sup> Nevertheless, the

comparison with our results is not direct since we do not use a direct measure of the orientation of the shear tidal tensor in the position of each galaxy and the radial direction of the voids can be considered only as a statistical proxy for the direction of the major principal axis of the shear tidal tensor. Given the differences in methodology, a meaningful comparison of the results from both works would need an analysis that it is beyond the scope of this paper.

## 6.2. Comparison with numerical simulations

Another way to study the alignment of galaxies with their local large scale environment is through numerical simulations (Porciani et al. 2002a,b; Navarro et al. 2004; Bailin & Steinmetz 2005; Bailin et al. 2005; Altay et al. 2006; Patiri et al. 2006b; Brunino et al. 2007; Aragón-Calvo et al. 2007; Cuesta et al. 2008; Zhang et al. 2009; Hahn et al. 2010; Bett et al. 2010). Since the behaviour of the halos can be dependent on the environment or the large scale structure in which they reside, to perform a meaningful comparison we have focused on the analysis done by Patiri et al. (2006b), Brunino et al. (2007) and Cuesta et al. (2008) in which it was studied the orientation of dark matter halos around cosmic voids using different cosmological simulations. The criteria imposed to the dark matter halos and the procedure to detect voids tried to match the criteria used in T06. All three works found that the minor axis and the major axis

<sup>13</sup>In the process of conducting this analysis we noted some duplications in a few galaxies that make the measured  $SNR$  decreases from 2.4 to 2.

<sup>14</sup>The authors obtained a value of  $c = 0.084 \pm 0.014$  which corresponds

to  $p = 1.057 \pm 0.012$

of the halos have significant tendencies to be aligned with the radial and the perpendicular directions, respectively. The results regarding the orientation of the angular momentum of the halos were less clear. Patiri et al. (2006b) did not find any particular orientation for the angular momentum of the halos. Brunino et al. (2007) also did not find any particular alignment for the angular momentum in their full sample of halos although they detected a tendency for those halos with a disc-dominated galaxy to have their angular momentum perpendicular to the radial direction. Finally, Cuesta et al. (2008) measured a significant ( $> 7\sigma$ ) tendency of the spin of the dark matter halos to lie in the plane perpendicular to the radial direction. However, the same authors found that the strength of the alignment is mainly produced by the outer regions of the DM halos and this would explain the discrepancies with Brunino et al. (2007) where the inner regions of the DM were used to measure the alignment.

How these results relate with ours is not straightforward since we observe the collapsed baryonic matter and they studied the dark matter or the non-collapsed baryonic matter. We can only point out the fact that the alignment that we find in the galaxies is shared by the minor axis of the halos studied in the simulations, either dark matter or gas halos. This is suggestive to an interaction between the galaxy and the hosting halos around it (either of dark or baryonic matter) leading to a tendency of the minor axis of the galaxy (and, therefore, its angular momentum) to be aligned with the minor axis of the halo's matter distribution.

## 7. Summary

Analysing a volume of  $\sim 27 \times 10^6 (h^{-1} \text{Mpc})^3$  from the SDSS-DR7 we have searched for cosmic voids devoid of galaxies brighter than  $M_r - 5 \log h = -20.17$  and with  $R_{\text{Void}} > 10 h^{-1} \text{Mpc}$ . We have found 699 non-overlapping voids for which we provide positions and sizes.

We have used this catalog of voids to search for disk galaxies around them and study the alignment between the direction of the angular momentum of these galaxies and the radial direction with respect to the center of the voids.

We have included two improvements with respect to previous similar works.

First, we have used an updated version of the SDSS spectroscopic catalog (data release 7) and we have combined it with the visual morphological classifica-

tion from the Galaxy Zoo project to get a reliable sample of disk galaxies.

Second and more important, we have introduced a statistical procedure that has allowed us to overcome the problem of the indetermination of the real inclination of galaxies computed from their apparent axial ratio. We have performed extensive Monte Carlo simulations to check the validity of this procedure. We show that the procedure recovers the real signal without practically any bias and its power in terms of capacity to reject the null hypothesis is equivalent to the case in which it is used a sample with complete knowledge of the real direction of the spin of the galaxies using 60% the amount of galaxies. In comparison with the common procedure of selecting only edge-on and face-on galaxies, this procedure means an increase of about a factor 3 in the amount of measurements used in the analysis of the alignment.

These improvements have allowed us to detect a statistically significant ( $\geq 98.8\%$ ) tendency of galaxies around very large voids ( $R \gtrsim 15 h^{-1} \text{Mpc}$ ) to have their angular momentum align with the radial direction of the voids. However, for smaller voids this tendency disappears and the results are consistent with no special alignment.

We have also found that the strength of the alignment depends on the distance of the galaxies to the surface of the voids and for galaxies further than  $\sim 5 h^{-1} \text{Mpc}$  the distribution of the alignments is compatible with a random distribution independent of the size of the voids.

Previous similar works found opposite alignment (T06) or no alignment (S09). However, these works used too few galaxies around voids with  $R \geq 10 h^{-1} \text{Mpc}$  which, according to our work, could mask the signal. In fact, using the same criteria for the size of the voids and the width of the shells as in those works, our data is compatible with a random distribution of spins without any particular alignment, as found by S09.

The comparison with the results from cosmological simulations points to a possible connection between the alignment of the halos (of dark matter and non-collapse baryonic matter) and that of the galaxies which could explain the similar orientation of both components observed in the simulations and in our work, respectively.

## REFERENCES

Adams, M. T., Strom, K. M., & Strom, S. E. 1980,



- ApJ, 238, 445
- Adelman-McCarthy, J. K., Agüeros, M. A., Allam, S. S., et al. 2008, ApJS, 175, 297
- Altay, G., Colberg, J. M., & Croft, R. A. C. 2006, MNRAS, 370, 1422
- Aragón-Calvo, M. A., van de Weygaert, R., Jones, B. J. T., & van der Hulst, J. M. 2007, ApJ, 655, L5
- Bailin, J., Kawata, D., Gibson, B. K., et al. 2005, ApJ, 627, L17
- Bailin, J. & Steinmetz, M. 2005, ApJ, 627, 647
- Banerji, M., Lahav, O., Lintott, C. J., et al. 2010, MNRAS, 406, 342
- Betancort-Rijo, J. E. & Trujillo, I. 2009, ArXiv e-prints
- Bett, P., Eke, V., Frenk, C. S., Jenkins, A., & Okamoto, T. 2010, MNRAS, 404, 1137
- Blanton, M. R., Schlegel, D. J., Strauss, M. A., et al. 2005, AJ, 129, 2562
- Brunino, R., Trujillo, I., Pearce, F. R., & Thomas, P. A. 2007, MNRAS, 375, 184
- Cuesta, A. J., Betancort-Rijo, J. E., Gottlöber, S., et al. 2008, MNRAS, 385, 867
- Dekel, A. 1985, ApJ, 298, 461
- Flin, P. & Godlowski, W. 1986, MNRAS, 222, 525
- Garrido, J. L., Battaner, E., Sanchez-Saavedra, M. L., & Florido, E. 1993, A&A, 271, 84
- Hahn, O., Teyssier, R., & Carollo, C. M. 2010, MNRAS, 405, 274
- Haynes, M. P. & Giovanelli, R. 1984, AJ, 89, 758
- Helou, G. & Salpeter, E. E. 1982, ApJ, 252, 75
- Kashikawa, N. & Okamura, S. 1992, PASJ, 44, 493
- Lee, J. 2004, ApJ, 614, L1
- Lee, J. & Erdogdu, P. 2007, ApJ, 671, 1248
- Lee, J. & Pen, U. 2000, ApJ, 532, L5
- Lintott, C., Schawinski, K., Bamford, S., et al. 2010, ArXiv e-prints
- Navarro, J. F., Abadi, M. G., & Steinmetz, M. 2004, ApJ, 613, L41
- Padmanabhan, N., Schlegel, D. J., Finkbeiner, D. P., et al. 2008, ApJ, 674, 1217
- Patiri, S. G., Betancort-Rijo, J. E., Prada, F., Klypin, A., & Gottlöber, S. 2006a, MNRAS, 369, 335
- Patiri, S. G., Cuesta, A. J., Prada, F., Betancort-Rijo, J., & Klypin, A. 2006b, ApJ, 652, L75
- Porciani, C., Dekel, A., & Hoffman, Y. 2002a, MNRAS, 332, 325
- Porciani, C., Dekel, A., & Hoffman, Y. 2002b, MNRAS, 332, 339
- Schäfer, B. M. 2009, International Journal of Modern Physics D, 18, 173
- Slosar, A. & White, M. 2009, J. Cosmology Astropart. Phys., 6, 9
- Strauss, M. A., Weinberg, D. H., Lupton, R. H., et al. 2002, AJ, 124, 1810
- Trujillo, I., Carretero, C., & Patiri, S. G. 2006, ApJ, 640, L111
- Zhang, Y., Yang, X., Faltenbacher, A., et al. 2009, ApJ, 706, 747

## A. Statistical computation of $P(|\cos \theta|)$ with full information

In this Appendix we describe in detail the statistical procedure that has been used to compute the corrected value of  $p$  using all the disk galaxies, independently of their inclination. We also show its validity and robustness using Monte Carlo simulations.

### A.1. Mathematical justification of the procedure

In the analysis of the alignment of galaxies, one of the main sources of uncertainty is the indetermination in the inclination of the plane of a disk galaxy with respect to the line of sight  $\pm\zeta$  using exclusively the observed axial ratio  $b/a$  of the galaxies (see Equation 1). In other words, if a galaxy is divided in two halves separated by its major axis, it is not possible to know which of the two halves is the closest to the observer.<sup>15</sup> This indetermination is negligible for edge-on ( $b/a \sim 0$ ) and face-on galaxies ( $b/a \sim 1$ ) but using only these galaxies reduces the sample size to  $\sim 1/5$  of the original one. As we increase the range of allowed values of  $b/a$ , the increasing uncertainties in  $\zeta$  will result in an increasing degradation of any existing alignment but the statistics improve. The question is whether this improvement of the statistics can compensate for the increasing degradation of any possible signal. The answer is “yes”. Choosing always the plus sign in the computation of  $\zeta$ , or the minus sign, or any random assignment of signs, leads to the same statistical results (i.e. they are equally powerful tests), which are better than those obtained with any limitation of the range of possible values of  $b/a$ . However, the estimate of the alignment obtained in this manner is biased towards smaller values (the strength of the alignment is given by  $(1 - p) \simeq -3c/4$  for weak alignments). This would not be much of a problem, because one may calibrate the procedure using Monte Carlo simulations and then correct for the biasing. In this manner we have found (see Table 7):

$$1 - p_+ \simeq 0.6(1 - p) \quad (\text{A1})$$

where  $p$  corresponds to the real alignment and  $p_+$  is the value obtained using the plus sign for  $\zeta$ .

The main problem with the use of  $p_+$ , or any other sign assignment, is that it introduces an artificial randomness that increases the scatter of the estimates. Using  $p_+$ , we assign the correct sign to half of the galaxies, on average, while the other half gets the wrong sign, but the exact number of galaxies getting the correct sign fluctuates from sample to sample (with variance  $N_g/4$ , being  $N_g$  the size of the sample) resulting in an increased error. Furthermore, since we do not take into account the other possible sign assignment, we do not know how large is the degradation of the alignment implied by those galaxies that get the wrong sign.

To avoid these problems we propose a method that uses all the information in the data and does not introduce artificial randomness. To this end, we consider the two possible values of  $\theta$  associated with every galaxy (one value for each possible sign of  $\zeta$ ) and assume that only half of the values of  $\theta$  falling in a given range are correct while the other half is incorrect. The correct values for the latter half of galaxies would be the conjugate of  $\theta$ ,  $\theta'$ , corresponding to the value of  $\theta$  using the opposite sign for  $\zeta$ . Thus, if the actual probability distribution for  $\theta$  were:<sup>16</sup>

$$\bar{P}(\cos \theta, p) = \frac{p}{(1 + (p^2 - 1) \cos^2 \theta)^{3/2}}, \quad (\text{A2})$$

the probability distribution that would be inferred from the  $2N_g$  values of  $\theta$  treating them as if they were independent,  $P(\cos \theta)$ , would be given, for the  $j - th$  bin, by:

$$P(\cos \theta_j) = \frac{1}{2} \bar{P}(\cos \theta_j, p) + \frac{1}{2l} \sum_{i=1}^l \bar{P}(\cos \theta'_i, p), \quad (\text{A3})$$

where  $l$  is the number of  $\theta_j$  values in the  $j - th$  bin.

<sup>15</sup>The use of kinematic information or the presence of dust lanes can help to break this indetermination, however, in most of the cases this information is not accessible.

<sup>16</sup>We are only interested in the direction of the alignment and therefore the analysis can be restricted to  $0 \leq \theta \leq \pi/2$  and  $\cos \theta = |\cos \theta|$ .

This formula expresses the fact that with probability 1/2, the probability density in the bin centered in  $\theta_j$  is given by the real distribution  $\bar{P}$  evaluated at  $\theta_j$  (correct sign assignment), while with probability 1/2, the probability density at  $\theta_j$  is the averaged of the value of  $\bar{P}$  over the conjugate values ( $\theta'_j(i)$ ) of the  $l$  values of  $\theta$  falling in bin  $j$ .

So, the factor:

$$Q(\cos \theta_j) \equiv \frac{\bar{P}(\cos \theta_j)}{\frac{1}{2}\bar{P}(\cos \theta_j, p) + \frac{1}{2l} \sum_{i=1}^l \bar{P}(\cos \theta'_j(i), p)} \quad (\text{A4})$$

is an estimate of the ratio between the actual distribution,  $\bar{P}(\cos \theta_j)$ , and the first estimate,  $P(\cos \theta_j)$ .

Therefore, we have for the estimate of  $\bar{P}$  (that we denote by  $P_c$ ):

$$P_c(\cos \theta_j) = P(\cos \theta_j)Q(\cos \theta_j) \quad (\text{A5})$$

When the alignment is very strong, the assumption that the two values  $\theta, \theta'$  of a conjugate couple have the same probability can no longer be maintained. Instead, we should used:

$$\text{Prob}(\theta) = \frac{P(\cos \theta)}{P(\cos \theta) + P(\cos \theta')} \quad (\text{A6})$$

$$\text{Prob}(\theta') = \frac{P(\cos \theta')}{P(\cos \theta) + P(\cos \theta')} \quad (\text{A7})$$

and modify the definition of  $Q$  consequently. However, this complication of the method is not worthy to our purpose. In fact, from Table 7, we can see that even for considerable alignment strengths, the bias implied by neglecting this last refinement is small, and can be corrected by the following expression:

$$p_{db} = 1 - (1 + 0.1(1 - p_c)^2)(1 - p_c) \quad (\text{A8})$$

where  $p_c$  is the value obtained using Equation (A5), and  $p_{db}$  is the debiased value.

From Table 7 we can also see that the relative error,  $\sigma_p/|1 - p|$ , is always larger for  $p_+$  or  $p_-$  than for  $p_c$ . For weak alignments ( $|1 - p| \lesssim 0.1$ ) the former is  $\sim 20\%$  larger than the latter, while for larger alignments the difference diminishes.

Finally, it must be noticed that the method that we have just described does not depend on the form of  $\bar{P}(\cos \theta)$ .

## A.2. Description of the procedure

In this appendix we describe the actual implementation of the method presented above.

The procedure is as follows:

1. For each galaxy, we compute the two possible values of  $\cos \theta$  corresponding to the two alternatives signs of  $\zeta$  and hence the two possible spin orientations.
2. Then, we construct a normalized histogram assuming the two values of  $\cos \theta$  of each galaxy as independent values. The normalization is done dividing each bin by 2 times the total number of galaxies of the sample ( $N_g$ ) and by the width of the bins. We call this non-corrected histogram  $P(\cos \theta)$ .
3. Next, in each bin centered in  $\cos \theta_j$ , we compute the value of the corrected histogram  $P_c(\cos \theta)$  using Equations (A5) and (A4):

$$P_c(\cos \theta_j) = P(\cos \theta_j)Q(\cos \theta_j) \quad (\text{A9})$$

remembering that

$$Q(\cos \theta_j) = \frac{\bar{P}(\cos \theta_j, p)}{\frac{1}{2}\bar{P}(\cos \theta_j, p) + \frac{1}{2l} \sum_{i=1}^l \bar{P}(\cos \theta'_j(i), p)}$$

and that  $\theta'_j(i)$  are the conjugate values of  $\theta$  for those galaxies with  $\theta_j(i)$  within the interval  $|\theta_j(i) - \theta_j| \leq \Delta\theta_j/2$ ,  $l$  is the total number of values within the bin, and

$$\bar{P}(\cos \theta, p) \equiv \frac{P}{(1 + (p^2 - 1) \cos^2 \theta)^{3/2}}. \quad (\text{A10})$$

The final corrected value of  $p$  is computed numerically using its relationship with  $\langle \cos \theta \rangle$  from Equation (8), which given the distribution  $P_c(\cos \theta_j)$  as a discrete distribution can be expressed as:

$$\frac{\sum_{j=1}^n P_c(\cos \theta_j) \cos \theta_j}{\sum_{j=1}^n P_c(\cos \theta_j)} = \frac{1}{1 + p} \quad (\text{A11})$$

with  $n$  the total number of bins in which the distribution is divided.

### A.3. Robustness of the statistical correction

To check the robustness of the statistical correction we have performed a series of Monte Carlo simulations. In these simulations, we use samples of fake galaxies in the position of the real ones but with spin directions assigned randomly following a  $p$  – *distribution* (Equations A2) with a given  $p_{input}$ . Then, the samples of fake galaxies are analysed in the same manner of the real galaxies and a final  $p_{output}$  value is obtained.

We have run 2 sets of simulations using two samples with different number of galaxies ( $N_g$ ) to check the robustness of the procedure also as a function of the sample size. These samples correspond to galaxies in shells of  $4 h^{-1}$  Mpc and  $R_{Void} > 10 h^{-1}$  Mpc (Sample A, following the usual criteria used in previous works) and to galaxies in shells of  $3 h^{-1}$  Mpc and  $R_{Void} > 16 h^{-1}$  Mpc (Sample B, corresponding to our maximum  $SNR$ ). For each sample we have run 1000 Monte Carlo realizations with 7 different initial distributions of  $\langle \cos \theta \rangle$  described by their corresponding  $p$  values ( $p_{input}$ ). These values covered the typical values of  $p$  that we have found in our analysis.

Table 7 shows the results of this analysis. For each subset of 1000 realizations we give the size of the sample  $N$ , the input value  $p_{input}$ , the mean value of  $p$  obtained if a fixed sign for  $\zeta$  is used ( $p_+$  and  $p_-$ , for plus and minor sign, respectively) and the mean value of  $p$  when applying our stastical correction,  $p_{output}$ . The uncertainties shown correspond to  $1\sigma$  of the distribution of the single values in the 1000 realizations.

We found that for most of the cases the statistically corrected value is within  $1\sigma$  of the input value showing the high accuracy of the procedure, especially when comparing with the cases in which a fixed sign is used.

The results of these simulations have been used to compute the “effective size” of the initial sample. This effective size is defined as the size that a sample with complete knowledge of the real signs of  $\zeta$  for each galaxy should have to show the same uncertainties that we find in our simulations. On what follows, it is described how we have computed the correction factor to be applied to our samples to obtain their effective sizes.

It can be proved theoretically that the value of the standard deviation of  $\langle \cos \theta \rangle$ ,  $\sigma_{\langle \cos \theta \rangle}$ , for the case in which there is no preferential alignment ( $p = 1$ ), is:

$$\sigma_{\langle \cos \theta \rangle} = \frac{1}{\sqrt{12N}}, \quad (\text{A12})$$

where  $N$  is the total number of galaxies used to compute  $\langle \cos \theta \rangle$ . However, this theoretical expression assumes the full knowledge of the values of  $\theta$  for all the galaxies, while empirically we do not have such full information because of the indetermination in the sign of  $\zeta$ . Therefore, we have compared the standard deviation obtained from the simulations with different values of  $N$ , with the theoretical value. From this comparison, we have obtained a correction factor to be applied to the total number of galaxies  $N$  equal to 0.6. This means that our statistical approximation carried an uncertainty that is equivalent to the uncertainty of having  $\sim 60\%$  of the galaxies with full information.

Sample	$N$	$p_{input}$	$p_+$		$p_-$		$p_{output}$	
			$\langle p_+ \rangle$	$\sigma_{p_+}$	$\langle p_- \rangle$	$\sigma_{p_-}$	$\langle p_{output} \rangle$	$\sigma_{p_{output}}$
A	11060	0.50	0.664	0.008	0.665	0.008	0.437	0.010
A	11060	0.75	0.841	0.010	0.842	0.009	0.746	0.012
A	11060	0.90	0.938	0.010	0.938	0.010	0.900	0.013
A	11060	1.00	1.000	0.011	1.000	0.011	1.000	0.014
A	11060	1.10	1.060	0.012	1.060	0.012	1.102	0.016
A	11060	1.25	1.143	0.012	1.142	0.012	1.256	0.018
A	11060	1.50	1.272	0.013	1.272	0.014	1.542	0.025
B	179	0.50	0.642	0.060	0.644	0.059	0.486	0.059
B	179	0.75	0.833	0.071	0.830	0.075	0.753	0.082
B	179	0.90	0.938	0.081	0.938	0.085	0.907	0.101
B	179	1.00	0.999	0.088	1.004	0.086	1.004	0.107
B	179	1.10	1.073	0.091	1.072	0.091	1.115	0.121
B	179	1.25	1.162	0.101	1.155	0.100	1.258	0.140
B	179	1.50	1.305	0.113	1.313	0.110	1.573	0.561

Table 7: Results of several simulations to test the validity and robustness of our statistical correction. Two samples with different number of galaxies are shown: Sample A is made of galaxies in shells of  $4 h^{-1}$  Mpc around voids with  $R > 10 h^{-1}$  Mpc and Sample B is made of galaxies in shells of  $3 h^{-1}$  Mpc around voids with  $R > 16 h^{-1}$  Mpc. Each row corresponds to a set of 1000 realizations in which to each real galaxy a synthetic spin vector was assigned following the theoretical distribution given by Equation (7) with a  $p = p_{input}$ .  $p_+$  and  $p_-$  are the values of  $p$  obtained when fixing the sign of  $\zeta$ .  $p_{output}$  is the final value after applying the statistical correction. For each parameter ( $p_+$ ,  $p_-$ ,  $p_{output}$ ), the mean and the standard deviation of the 1000 realizations are shown. See text for more details.

## B. Computation of the uncertainties in $\langle |\cos \theta| \rangle$ and $p$

In this section we present the expressions used to compute the uncertainties in  $\langle |\cos \theta| \rangle$  and  $p$ , in the general case.

The standard deviation of  $\langle |\cos \theta| \rangle$ ,  $\sigma_{\langle |\cos \theta| \rangle}$ , is computed as  $\sigma_{\langle |\cos \theta| \rangle} / \sqrt{N_g}$ , where  $N_g$  is the total number of galaxies.  $\sigma_{\langle |\cos \theta| \rangle}$  is the root mean square of  $|\cos \theta|$  for the distribution given by Equation 7. Computing  $\sigma_{\langle |\cos \theta| \rangle}$  analytically, we find the following expressions for  $\sigma_{\langle |\cos \theta| \rangle}$  depending on the value of  $p = \langle |\cos \theta| \rangle^{-1} - 1$ , :

$$\sigma_{\langle |\cos \theta| \rangle} = \frac{1}{\sqrt{N_g}} \sqrt{\frac{p}{(p^2 - 1)^{3/2}} \ln(p + \sqrt{p^2 - 1}) - \frac{1}{p^2 - 1} - \frac{1}{1 + p^2}}; \quad p > 1 \quad (\text{B1})$$

$$\sigma_{\langle |\cos \theta| \rangle} = \frac{1}{\sqrt{N_g}} \frac{1}{\sqrt{12}}; \quad p = 1 \quad (\text{B2})$$

$$\sigma_{\langle |\cos \theta| \rangle} = \frac{1}{\sqrt{N_g}} \sqrt{\frac{1}{1 - p^2} - \frac{p}{(1 - p^2)^{3/2}} \arcsin(\sqrt{1 - p^2}) - \frac{1}{1 + p^2}}; \quad p < 1 \quad (\text{B3})$$

When using the method described in Appendix A.3, we have some uncertainty in the direction of the spin, but we find that the errors are well described by the above expressions using 0.6 times the number of galaxies in the place of  $N_g$  (see Table 7).

Since the distribution of  $p$  is not Gaussian, we can compute the value  $p$  and the limits of the  $1\sigma$  confidence interval ( $p_{-\sigma}$ ,  $p_{+\sigma}$ ) with the next expressions:

$$p = \frac{1}{\langle |\cos \theta| \rangle} - 1 \quad (\text{B4})$$

$$p_{-\sigma} = \frac{1}{\langle |\cos \theta| \rangle + \sigma_{\langle |\cos \theta| \rangle}} - 1 \quad (\text{B5})$$

$$p_{+\sigma} = \frac{1}{\langle |\cos \theta| \rangle - \sigma_{\langle |\cos \theta| \rangle}} - 1 \quad (\text{B6})$$

This work has been supported by the Programa Nacional de Astronomía y Astrofísica of the Spanish Ministry of Science and Innovation under grant AYA2010-21322-C03-02. J.V. acknowledges a post-doc fellowship from the Spanish Ministry of Science and Innovation under the programs 3I2005 and 3I2406.

Funding for the SDSS and SDSS-II has been provided by the Alfred P. Sloan Foundation, the Participating Institutions, the National Science Foundation, the U.S. Department of Energy, the National Aeronautics and Space Administration, the Japanese Monbukagakusho, the Max Planck Society, and the Higher Education Funding Council for England. The SDSS Web Site is <http://www.sdss.org/>.

The SDSS is managed by the Astrophysical Research Consortium for the Participating Institutions. The Participating Institutions are the American Museum of Natural History, Astrophysical Institute Potsdam, University of Basel, University of Cambridge, Case Western Reserve University, University of Chicago, Drexel University, Fermilab, the Institute for Advanced Study, the Japan Participation Group, Johns Hopkins University, the Joint Institute for Nuclear Astrophysics, the Kavli Institute for Particle Astrophysics and Cosmology, the Korean Scientist Group, the Chinese Academy of Sciences (LAMOST), Los Alamos National Laboratory, the Max-Planck-Institute for Astronomy (MPIA), the Max-Planck-Institute for Astrophysics (MPA), New Mexico State University, Ohio State University, University of Pittsburgh, University of Portsmouth, Princeton University, the United States Naval Observatory, and the University of Washington.